Neurobiology of Aging 34 (2013) 1328–1342

Contents lists available at SciVerse ScienceDirect

Neurobiology of Aging

journal homepage: www.elsevier.com/locate/neuaging

# Cortical beta amyloid protein triggers an immune response, but no synaptic changes in the APPswe/PS1dE9 Alzheimer's disease mouse model

Kerstin T.S. Wirz [a,*], Koen Bossers [a,b], Anita Stargardt [a], Willem Kamphuis [c], Dick F. Swaab [b], Elly M. Hol [c,d], Joost Verhaagen [a,e]

[a] Laboratory for Neuroregeneration, Netherlands Institute for Neuroscience, An Institute of the Royal Netherlands Academy of Arts and Sciences, Amsterdam, The Netherlands
[b] Laboratory for Neuropsychiatric Disorders, Netherlands Institute for Neuroscience, An Institute of the Royal Netherlands Academy of Arts and Sciences, Amsterdam, The Netherlands
[c] Department of Astrocyte Biology and Neurodegeneration, Netherlands Institute for Neuroscience, An Institute of the Royal Netherlands Academy of Arts and Sciences, Amsterdam, The Netherlands
[d] Swammerdam Institute for Life Sciences, Center for Neuroscience, University of Amsterdam, The Netherlands
[e] Center for Neurogenomics and Cognitive Research, Neuroscience Campus Amsterdam, VU University, Amsterdam, The Netherlands

ARTICLE INFO

*Article history:*
Received 21 June 2012
Received in revised form 14 November 2012
Accepted 16 November 2012
Available online 12 December 2012

*Keywords:*
Alzheimer's disease
APPswe/PS1dE9 mice
Beta amyloid protein
Immune response
Microarray
Synaptic activity and plasticity

ABSTRACT

Using microarray technology we studied the genome-wide gene expression profiles in the frontal cortex of APPswe/PS1dE9 mice and age and sex-matched littermates at the age of 2, 3, 6, 9, 12, and 15–18 months to investigate transcriptional changes that are associated with beta amyloid protein (Aβ) plaque formation and buildup. We observed the occurrence of an immune response with glial activation, but no changes in genes involved in synaptic transmission or plasticity. Comparison of the mouse gene expression data set with a human data set representing the course of Alzheimer's disease revealed a strikingly limited overlap between gene expression in the APPswe/PS1dE9 and human Alzheimer's disease prefrontal cortex. Only plexin domain containing 2, complement component 4b, and solute carrier family 14 (urea transporter) member 1 were significantly upregulated in the mouse and human brain which might suggest a function in Aβ pathology for these 3 genes. In both data sets we detected clusters of upregulated genes involved in immune-related processes. We conclude that the APPswe/PS1dE9 mouse can be a good model to study the immune response associated with cortical Aβ plaques.


## 1. Introduction

Alzheimer's disease (AD) is the most common form of dementia among older people accounting for 60%–70% of all cases (World Health Organization and Alzheimer's Disease International, 2012). The disease is neuropathologically characterized by the presence of extracellular deposits of beta amyloid protein (Aβ) in senile plaques, intracellular deposits of hyperphosphorylated tau protein in neurofibrillary tangles, dystrophic neurites, and by neuropil threads (Braak et al., 1998). Besides the sporadic form of AD, for which aging is the main risk factor, mutations in amyloid precursor protein (APP), presenilin 1 (PSEN1), and presenilin 2 (PSEN2) have been found to cause autosomal dominant early onset familial AD in a small number of families (Bertram and Tanzi, 2005). The autosomal dominant form of AD is a very rare disorder with a prevalence less than 0.1% (Harvey et al., 2003). Most mutations in these 3 genes result in alterations in the level of Aβ in the brain and in the isoforms of Aβ being produced, leading to Aβ species with a higher propensity to aggregate. Introducing mutated forms of APP and PSEN1 individually or in combination into mice has led to the development of a variety of transgenic mouse lines that model aspects of Aβ pathology (Wisniewski and Sigurdsson, 2010). These mouse models have contributed significantly to our understanding of the molecular processes associated with plaque formation. It is, however, unclear whether the molecular alterations that cause plaque formation in models for familial AD also occur in nonfamilial, sporadic forms of AD. The suitability of current AD mouse models for studying sporadic AD therefore warrants further investigation.

We have recently performed a genome-wide gene expression study in the human prefrontal cortex during the progression of sporadic AD (Bossers et al., 2010a). One of the most important findings was a concerted increase of genes involved in synaptic transmission and plasticity in nondemented individuals, in the preclinical stages of AD, just before the onset of plaque pathology in the prefrontal cortex. In parallel, we observed an increase in intraneuronal Aβ levels. In contrast, after the development of the first plaques and tangles, the expression of these genes, which also

* Corresponding author at: Netherlands Institute for Neuroscience, Meibergdreef 47, 1105 BA Amsterdam, The Netherlands. Tel.: +31 (0)20 566 5512; fax: +31 (0)20 566 6121.
*E-mail address:* k.wirz@nin.knaw.nl (K.T.S. Wirz).

0197-4580 
http://dx.doi.org/10.1016/j.neurobiolaging.2012.11.008

include a group of genes involved in the generation and breakdown of Aβ, sharply decreased. At the same time patients show memory impairments. Thus, we hypothesize that the initial increase in synaptic transmission and plasticity represents a compensatory reaction to the earliest Aβ-related changes in AD.

Our gene expression data in AD provide the unique opportunity to examine whether similar changes in synaptic activity and plasticity can also be observed in Aβ-based AD mouse models. We therefore have generated genome-wide expression profiles from the frontal cortex of APPswe/PS1dE9 transgenic mice (Jankowsky et al., 2004) and from their nontransgenic littermates throughout the entire progression of Aβ pathology from 2 to 18 months of age. This double-transgenic mouse coexpresses APP695 with the Swedish mutation (K594M/N595L) and the human exon-9-deleted variant of PSEN1 and develops Aβ plaques before 6 months of age (Jankowsky et al., 2004). These mice also manifest memory deficits as early as the age of 2 months (Bonardi et al., 2011; Jankowsky et al., 2005; O'Leary and Brown, 2009; Pillay et al., 2008; Savonenko et al., 2005).

Surprisingly, our gene expression data show that plaque formation and buildup in the frontal cortex of APPswe/PS1dE9 mice is solely associated with an increased expression of genes involved in an immune response and in glial activation, and in this brain region does not cause any changes in genes associated with memory, synaptic transmission, and plasticity.

## 2. Methods

### 2.1. Animals

In this study we used the double transgenic APPswe/PS1dE9 mouse, line 85 (Jankowsky et al., 2004). For details see The Jackson Laboratory (strain B6C3-Tg(APPswe,PSEN1dE9)85Dbo/J; stock number 004462; http://jaxmice.jax.org/). These animals express chimeric mouse/human APP695 with the Swedish mutation (K594M/N595L) and the human exon-9-deleted variant of PS1 (PS1dE9) under independent mouse prion protein promoters. AD mice were maintained as hemizygous and crossed with wild type (WT) C57BL/6. Genotyping was performed by real-time polymerase chain reaction (PCR) assays specific for the 2 transgenes and the prion promotor. All animals were housed under standard conditions with access to water and food ad libitum. For microarray and quantitative PCR (qPCR) experiments, 3 male and 3 female transgenic APPswe/PS1dE9 mice were used at each age (2, 3, 6, 9, 12, and 15–18 months) studied. WT littermate mice served as age- and sex-matched control animals (2 male, 2 female per age group). For immunoblot analysis, additional APPswe/PS1dE9 mice at the age of 3 ($n = 2$), 6 ($n = 3$), 9 ($n = 1$), and 18 ($n = 3$) months were used. Immunohistochemistry was performed on animals also used for microarray, qPCR, or immunoblot studies. Animal handling and experimental procedures were reviewed and approved by the ethical committee for animal care and use of experimental animals of the Royal Netherlands Academy for Arts and Sciences, acting in accordance with the European Community Council directive of November 24, 1986 (86/609/EEC). All efforts were made to minimize suffering and number of animals used for the study presented here.

### 2.2. Tissue harvesting

Animals were anesthetized with $CO_2/O_2$ and decapitated. The gray matter of the right frontal cortex was isolated, snap-frozen in liquid nitrogen, and stored at −80 °C for subsequent RNA or protein isolation. The left hemisphere was immersion fixed in phosphate-buffered 4% paraformaldehyde (PFA/PBS, pH 7.4) overnight at 4 °C. After fixation the tissue was cryoprotected in phosphate buffered saline (PBS) containing 20% sucrose for a minimum of 5 hours at 4 °C, embedded in Tissue-Tek (Sakura Finetek Europe, Alphen aan de Rijn, the Netherlands), frozen on dry ice, and stored at −80 °C to be used for immunohistochemical analysis.

### 2.3. RNA isolation

RNA was isolated using a combination of TRIzol (Invitrogen Life Technologies, Carlsbad, CA, USA)-based and RNeasy Mini Kit (Qiagen, Hilden, Germany) RNA isolation methods. Briefly, frozen cortex tissue was homogenized in ice-cold 500 μL TRIzol and centrifuged at 12,000 *g* for 10 minutes. The supernatant was transferred to a new tube and vigorously mixed with 100 μL chloroform. Samples were loaded onto a Phase Lock Gel tube (5 Prime, Hamburg, Germany) and centrifuged at 12,000 *g* for 15 minutes. The aqueous phase was collected, mixed with an equal amount of 70% ethanol, applied to an RNeasy spin column and further processed according to the manufacturer's instructions. RNA was eluted in RNase-free water and stored at −80 °C. RNA purity and yields were determined by a NanoDrop ND-1000 spectrophotometer (NanoDrop Technologies, Wilmington, DE, USA). RNA integrity was determined by the RNA integrity number, as measured by the Agilent 2100 bioanalyzer (Agilent Technologies, Palo Alto, CA, USA). The isolated RNA was of high integrity (average RNA integrity number 8.7, ranging from 7.3–9.5).

### 2.4. RNA labeling and microarray hybridization

For microarray analysis, the Whole Mouse Genome Microarray Kit with 4 × 44000 probes was used (Agilent Technologies, Part Number G4122F). RNA labeling and microarray hybridization were performed according to the manufacturer's instructions. In short, for each sample 1 μg total RNA was linearly amplified and fluorescently labeled with either Cy3- or Cy5-cytosine triphosphate using the Agilent Low RNA Input Fluorescent Linear Amplification Kit (Agilent Technologies). Before hybridization, equal amounts (825 ng) of Cy3-labeled and Cy5-labeled complementary RNA were mixed and fragmented in 1× fragmentation buffer (Agilent Technologies) at 60 °C for 30 minutes. The sample mix was hybridized to a microarray in 1× Hi-RPM Hybridization Buffer (Agilent Technologies) at 65 °C for 17 hours in a rotating hybridization chamber. A detailed description of all hybridizations for both the transgenic and wild type animals can be found in Supplementary Fig. 1.

After hybridization, microarrays were washed in 6× saline sodium phosphate-EDTA (SSPE)/0.005% N-Lauroylsarcosine for 5 minutes (Sigma-Aldrich, St. Louis, MO, USA), in 0.06x SSPE/ 0.005% N-Lauroylsarcosine for 1 minute and acetonitrile (Sigma-Aldrich) for 30 seconds, then dried in a nitrogen flow.

The microarrays were scanned with an Agilent DNA Microarray scanner at 100% photomultiplier tube setting and 5 μm resolution. Microarray scans were quantified using Agilent Feature Extraction software (version 9.5.3).

### 2.5. Microarray normalization and single gene analysis

Raw expression data were analyzed in R statistical processing software (version 2.6.0) using the LIMMA package (Smyth, 2004) in Bioconductor (http://www.bioconductor.org). All features that were flagged as saturated or as a nonuniformity outlier by the feature extraction software on 1 or more arrays were excluded from further analysis. This was applicable for 2039 features, resulting in 39,136 features which passed these criteria. Data were normalized using LIMMA by applying a background correction (using the 'normexp' algorithm) followed by normalization of intensity distributions within and between arrays (using the 'quantile' algorithm). We have recently demonstrated that the analysis of the separate intensity

channels (the individual Cy3 and Cy5 signals) yields more reproducible results than the standard ratio-based approach (the ratio between the Cy3 and Cy5 channels) for dual-color microarray datasets (Bossers et al., 2010b), so we also applied this approach for the present dataset. Thus, the $^2$log-transformed intensity measurements per sample were extracted from the normalized ratio data and used in all following analyses.

To detect genes with a significant interaction between age and genotype, we performed a 2-way analysis of variance (ANOVA) using age and genotype as grouping factors. The Benjamini–Hochberg method was used to correct for multiple testing. $p$-values $< 0.05$ after correction were considered significant. A separate analysis for differences between genotypes in each age group using Student $t$ tests revealed very similar differentially regulated genes as the ANOVA and is, therefore, not further considered here.

### 2.6. Cluster analysis of gene expression profiles

To follow the expression of individual transcripts over time we constructed time profiles of each transcript per genotype. Specifically, for each transcript, mean expression values for each age group were determined by averaging the individual intensity measurements. Expression values were normalized against the mean expression of all 2-month-old animals. Cluster analysis was performed to detect groups of transcripts with similar expression profiles (fuzzy clustering with the Mfuzz package, version 2.6.1 in Bioconductor). The fuzziness parameter M was determined by optimizing the detection of clusters as described in the Mfuzz manual, resulting in an M value of 1.3 that was used for further analysis. The microarray expression dataset was clustered into 8 separate clusters that allowed for the detection of small differences in expression profiles between gene clusters.

### 2.7. GO analysis of gene clusters

To gain insight into the biological functions that are associated with the gene clusters, overrepresented Gene Ontology (GO) classes associated with these clusters were determined with the GoStat program (http://gostat.wehi.edu.au) (Beißbarth and Speed, 2004), using all genes on the array as a background dataset. GoStat output was corrected for multiple testing with the Benjamini–Hochberg method. The first 30 GO classes with a $p$ value $< 0.001$ which contained more than 5 genes, for which at least 1 gene was represented in the cluster under investigation, are presented in the final results (Table 2). GoStat does not allow for an evaluation of whether a significant 'parental branch' can be solely explained by its children.

### 2.8. Ingenuity pathway analysis of regulated genes

We performed a pathway analysis for all genes from cluster 4 and 8 (the clusters that showed a strong expression regulation over time). Ingenuity Pathway Analysis software (version 7.6; Ingenuity Systems, Mountain View, CA, USA) was used to identify direct and indirect physical and/or functional interactions between genes and/or their protein products. To keep the results relevant for Aβ deposition and AD related processes we included only significantly enriched canonical pathways in the final results table which were not related to a specific disease and contained at least 3 molecules.

### 2.9. Real-time qPCR confirmation

All qPCR experiments were performed on the same animals that were used for the microarray study. The time points 2, 3, 6, 9, 12, and 15–18 months were evaluated. For each sample 1 μg total RNA was reverse transcribed using the QuantiTect Reverse Transcription Kit (Qiagen) according to the manufacturer's protocol. As negative control, samples of each batch of reverse transcription were pooled and incubated with primer mix lacking reverse transcriptase. The obtained cDNA was stored at −20 °C until use. Primers were designed using Primer3 (http://frodo.wi.mit.edu) (Rozen and Skaletsky, 2000). Primer sequences are listed in Supplementary Table 1. For each primer pair, dissociation curves were generated to assess specificity. Only single products and no primer dimers were detected. Each qPCR reaction contained 1.5 μL 2 μM primer solution, 5 μL SYBR Green Master mix (Applied Biosystems) and 2.86 ng cDNA in a 10 μL reaction volume. The reaction was run at default settings (95 °C, 15 seconds; 60 °C, 1 minute; 40 cycles) on the ABI Prism 7300 sequence detection system (Applied Biosystems). Samples were normalized to the housekeeping genes 28S, Gapdh, and β-actin that are not regulated between different ages in the mice used. Normalization factors were determined using the GeNorm (Vandesompele et al., 2002) VBA applet (version 3.5) for Microsoft Excel.

### 2.10. Immunohistochemistry

Ten-μm cryostat sections were mounted on Superfrost Plus slides (Thermo Scientific Menzel, Braunschweig, Germany). Sections were stored at −80 °C or −20 °C until use. Cryosections were dried for 15 minutes and fixed in 4% PFA/PBS (pH 7.4) for 3 minutes. Antigen retrieval was performed in 10 mM sodium citrate (pH 6.0)/0.05% Tween-20 for 20 minutes at 95 °C. For the immunohistochemical detection of Aβ, an additional pretreatment with 70% formic acid for 10 minutes was performed. Sections were then blocked with 10% fetal calf serum (FCS) in PBS/0.4% Triton-X 100 for 1 hour at room temperature. Thereafter, sections were incubated with monoclonal antibody 4G8 (Signet Laboratories, Dedham, MA, USA; 1:10,000) in PBS/0.4% Triton-X 100 for 1 hour at room temperature. Next, sections were incubated with biotinylated horse anti-mouse antibody (Vector Laboratories, Burlingame, CA, USA; 1:400) in PBS/1% FCS for 1 hour at room temperature. Sections were incubated in ABC solution (Vector Laboratories) for 1 hour at room temperature, followed by a 5-minute incubation with 3,3'-diaminobenzidine as chromogen. Sections were dehydrated in a graded ethanol series followed by xylene and embedded with entellan glue. For quantification of Aβ load, tiled photographs of the whole section were taken with a XC-77CE CCD monochrome camera (Sony, Badhoevedorp, The Netherlands) through a 10× objective connected to an Axioskop microscope (Zeiss, Jena, Germany). Analysis of the cortex area covered with Aβ plaques was done using the Image-Pro Plus software (version 6.0, Media Cybernetics, Bethesda, MD, USA) with a computer-generated mask manually overlaid on the cortex, which recognized 3,3'-diaminobenzidine staining. Plaque load was evaluated in all animals used for the microarray and qPCR studies.

For immunofluorescent stainings of glial-fibrillary acidic protein (GFAP), allograft inflammatory factor 1 (IBA1), and complement component 4b (C4B), cryostat sections of 3- and 15–18-month-old animals were used (4 transgenic animals per age group: 4 males at 3 months, 2 males and 2 females at 15–18 months; 2 WT male animals per age group). Tissue from 6 transgenic animals and the WT animals were also used in the microarray study; tissue from 2 transgenic animals was used in the immunoblot experiments. Fixation and retrieval were performed as described above. Primary antibodies were rabbit anti-C4B (Abcam, Cambridge, UK; 1:300), rabbit anti-IBA1 (Wako Chemicals, Neuss, Germany; 1:600) and rabbit anti-GFAP (Dako, Glostrup, Denmark; 1:2000) in PBS/0.4% Triton-X 100/3% FCS overnight at 4 °C. Cy3-conjugated donkey anti rabbit IgG (Jackson Immuno Research, Newmarket, Suffolk, UK; 1:1000) in PBS/0.4% Triton-X 100/1% FCS was used as secondary antibody for 2 hours at room temperature. Aβ plaques were

visualized with 0.0125% thioflavine S in 50% ethanol for 10 minutes. Sections were then treated with Hoechst (Invitrogen; 1:20,000) in PBS for 10 minutes to visualize cell nuclei and mounted with Mowiol embedding medium. Photographs were taken using an Axioplan 2 fluorescent microscope (Zeiss) connected to an MP digital camera (MediaCybernetics) with a 20× objective.

### 2.11. Western blot analysis

The frozen right hemisphere cortex samples were homogenized in suspension buffer (0.1 M NaCl, 0.01 M Tris-HCl, 0.001 M ethylenediaminetetraacetic acid) containing protease inhibitors (20 mM antipain, 1 mM pepstatin, 20 mM chymostatin, 10 mg/mL leupeptin, and 100 mg/mL phenylmethanesulphonylfluoride) using an ultra turrax tissue homogenizer. Homogenates were centrifuged at 14,000 rpm for 5 minutes at 4 °C, the supernatant was collected and protein concentrations were measured using a bicinchoninic acid protein assay kit (Pierce, Thermo Scientific, Rockford, IL, USA). Immunoblotting experiments were performed for GFAP, C4B, and IBA1 using the same antibodies as for the immunostainings. For each sample, 26.8 μg protein was heated in 5× loading buffer containing 10% sodium dodecyl sulphate and 10% β-mercaptoethanol at 95 °C for 10 minutes. Tris-glycine sodium dodecyl sulphate polyacrylamide gel electrophoresis was performed using the BioRad Mini-PROTEAN 3 gel electrophoresis system (Bio-Rad Laboratories, Hercules, CA, USA). Gels contained 8% (C4B), 12% (GFAP), and 15% (IBA1) acrylamide/bisacrylamide. Proteins were transferred to nitrocellulose membranes using a semidry (GFAP and IBA1) or wet (C4B) blotting procedure and blocked with 5% fat-free milk powder in PBS/0.05% Tween-20 for 1 hour at room temperature. Blots were incubated with antibodies against GFAP, C4B (diluted in PBS/0.05% Tween-20/5% milk) or IBA1 (diluted in supermix: 0.25% gelatin, 0.5% Triton-X 100 in PBS, pH 7.4) for 2 hours at room temperature or 4 °C overnight. β-actin (Sigma-Aldrich; 1:2000) was used as a loading control. Primary antibodies were detected with an IR800 antibody (Rockland Immunohistochemicals, Gilbertsville, PA, USA; 1:5000) and β-actin was detected with a Cy5-conjugated antibody (Jackson Immuno Research; 1:2000) for 2 hours at room temperature. Blots were scanned and analyzed using the Odyssey Infrared Imager and Odyssey 2.1 scanning software (LI-COR Biosciences, Lincoln, NE, USA). The β-actin signal was used to normalize the final protein quantifications.

## 3. Results

### 3.1. Aβ plaque pathology in APPswe/PS1dE9 mice increases with age

We first confirmed the previously documented plaque pathology in our mouse colony. Immunohistochemical detection of Aβ, using the 4G8 antibody, in brain sections of the APPswe/PS1dE9 transgenic mice showed that Aβ plaque load in the frontal cortex increased with age (Fig. 1). The first plaques were detected at the age of 6 months. This is in good agreement with earlier reports showing that these mice show plaques from very early in age (Garcia-Alloza et al., 2006; Jankowsky et al., 2004; Kamphuis et al., 2012; Ruan et al., 2009). As the plaque load in the frontal cortex of APPswe/PS1dE9 mice did not change between 15 and 18 months of age (3.61 ± 0.5% vs. 3.65 ± 1.2%; $p > 0.05$), we combined these 2 age groups for the gene expression analysis.

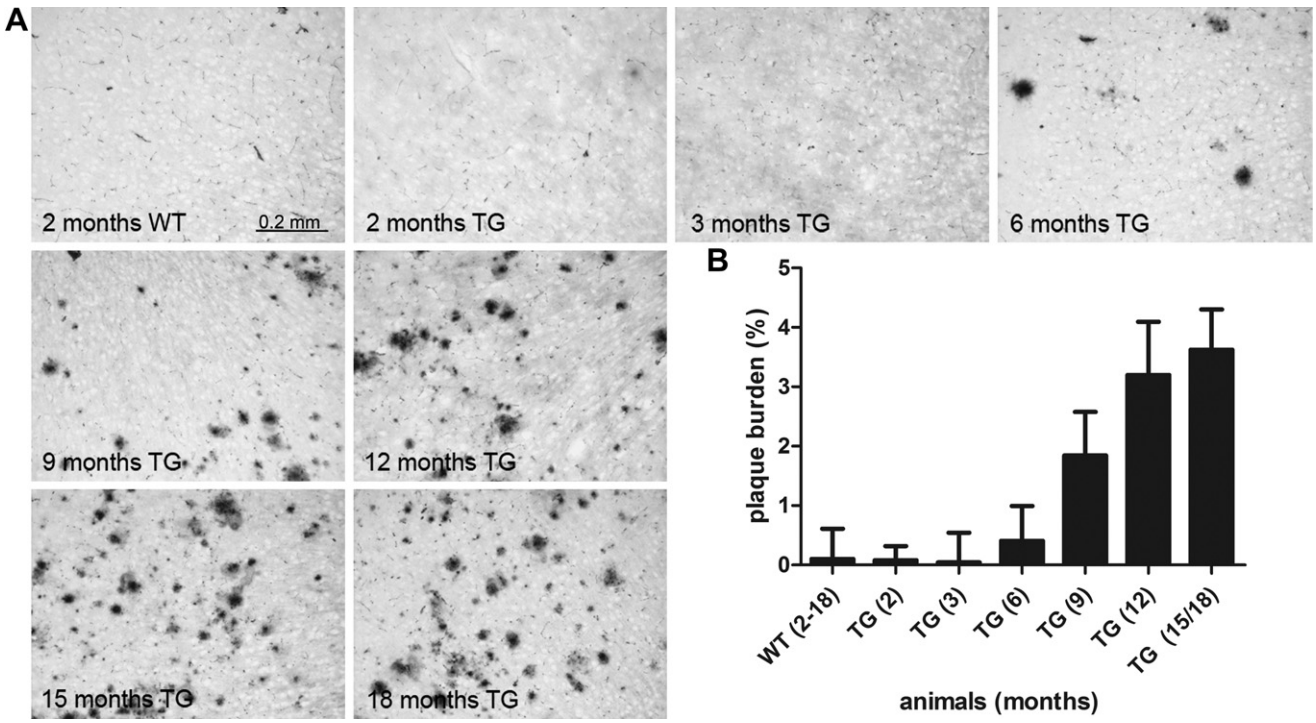


**Fig. 1.** Beta amyloid protein (Aβ) plaque pathology increased with age in APPswe/PS1dE9 mice. (A) Aβ plaques were stained with the monoclonal anti-amyloid 4G8 antibody on the left hemisphere of the frontal cortex. First plaques were detected at 6 months of age and plaque burden increased with age. A representative example picture of a 2-month-old wild type mouse cortex (upper left), is shown together with representative examples from APPswe/PS1dE9 transgenic mice at the age of 2, 3, 6, 9, 12, 15, and 18 months. Scale bar: 0.2 mm. (B) Quantification of plaque load in the frontal cortex of APPswe/PS1dE9 and wild type mice for all age groups ($n = 6$ per group). Plaque load is represented in percentage of the frontal cortex area that is covered with plaques. The increase of plaque load over time is significant (analysis of variance; $p < 0.001$). Wild type animals do not show increased plaque load with age and are pooled for the quantification. Abbreviations: TG, transgenic; WT, wild type.

### 3.2. Microarray analysis of gene expression: upregulation of genes coincides with plaque development

To determine the gene expression changes that are specifically associated with Aβ pathology, microarrays were used to assess the transcriptional alterations that occur during the development of plaque pathology in the frontal cortex of APPswe/PS1dE9 mice, and we compared these with age-related gene expression changes in age-matched wild type littermates. A total of 87 transcripts showed a significant interaction between age and genotype (ANOVA-based $p$ value $< 0.05$, Table 1). All significantly regulated transcripts were upregulated over time. No genes were detected that showed a transcriptional downregulation with age and plaque development. Among the significantly upregulated genes were many genes involved in the regulation of immune function such as a large group of Cluster of differentiation (Cd) antigens (Cd9, Cd14, Cd48, Cd52, Cd68, Cd84, Cd86, Cd180, Cd300d, Cd300lf, Fcgr2b, Fcgr3, Itgax, Lair1, Lilrb4, Pdcd1, Siglecf, Tlr2, Tnfsf13b), chemokine ligands (Ccl3, Ccl4, Ccl6, Cxcl5), and members of the complement system (C1qc, C4b). The microglia marker allograft inflammatory factor 1 (Aif1/Iba1) and the astrocyte marker glial fibrillary acidic protein (Gfap) were 2.2- and 7.9-fold upregulated, respectively. Furthermore, we found genes involved in lipid metabolism (Apobec1, Apoc4, Ch25h, Lpl) and cathepsins (Ctsc, Ctsh, Ctsz) to be upregulated.

Next, we performed a cluster analysis on the expression profiles of all genes over time in both the APPswe/PS1dE9 transgenic animals and in wild type controls to detect groups of genes with concerted patterns of expression. In the APPswe/PS1dE9 mouse, this cluster analysis revealed 2 clusters (4 and 8) in which transcripts showed an upregulation starting between 3 and 6 months of age; coinciding with the development of Aβ plaque pathology (Fig. 2A). Cluster 8 contained the transcripts with the highest fold changes. Transcripts in cluster 4 also showed a continuous upregulation over time but with lower fold changes. Before the onset of plaque pathology, at the 2- and 3-month time points, no gene regulation was detected. Clusters of transcripts of wild type animals did not show any significant changes in their time profile (data not shown).

We selected a set of 17 regulated genes (Bcl3, synaptogyrin 1 [Syngr1], Baiap2l2, Birc1b, activating transcription factor 3 [Atf3], Itgax, Pdcd1, Ccl6, Gpr109a, Tlr2, Trem2, Iba1, Tyropb, Cd9, Bcl2a1b, Igf1, Gfap) to validate the microarray data using qPCR. For all selected genes the patterns of gene expression over time were highly correlated between the microarray and qPCR measurements ($R^2 \geq 0.96$; $p < 0.001$; example plots see Fig. 2B) for the APPswe/PS1dE9 mice. Furthermore, fold change between APPswe/PS1dE9 and wild type at 15–18 months as measured by qPCR showed a strong linear correlation with the microarray-derived fold change at that same time point ($R^2 = 0.85$; $p < 0.001$; Fig. 2C).

### 3.3. Functional annotation and pathway analysis: immune response is induced after plaque formation

To investigate which biological processes were associated with the upregulated genes in APPswe/PS1dE9 mice, we performed a GO overrepresentation analysis on the upregulated clusters 4 and 8. This analysis revealed that these clusters were highly enriched for transcripts involved in immune response-associated processes, such as the biological process GO classes 'immune system process,' 'defense response,' 'response to external stimulus,' and 'response to wounding and inflammatory response' (see Table 2 for the 30 most significant GO identifiers and Supplementary Table 2 for the complete list [$p < 0.01$]). Overrepresented cellular component GO classes were among others 'cell surface,' 'MHC I and II protein complex,' and 'lysosome'. Prominent overrepresented GO classes of molecular function were 'immunoglobulin binding,' and 'chemokine and cytokine activity.'

In addition to the GO overrepresentation analysis we performed an Ingenuity Pathway analysis on the upregulated clusters 4 and 8. The canonical pathways that were significantly enriched included Dendritic Cell Maturation, Role of Pattern Recognition Receptors in Recognition of Bacteria and Viruses, T Helper Cell Differentiation, Antigen Presentation Pathway and Communication between Innate and Adaptive Immune Cells (see Supplementary Table 3 for the full list of overrepresented pathways). The results of the Ingenuity Pathway analysis and GO analysis were thus in general agreement with each other.

### 3.4. IBA1, GFAP, and C4B protein levels corroborate the gene expression data

Gene expression data indicated an immune and glial response in APPswe/PS1dE9 mice including the upregulation of Iba1, Gfap, and complement component 4b (C4b). We therefore studied whether microgliosis, astrogliosis, and inflammation were also present on the protein level using antibodies against IBA1, GFAP, and C4B, respectively. Analysis of the immunoreactivity levels revealed that IBA1, GFAP, and C4B protein were highly upregulated in the frontal cortex of APPswe/PS1dE9 mice at 15 months of age (when plaques were abundantly present) compared with age-matched wild type animals without plaque pathology (Fig. 3A). GFAP staining was observed in activated astroglia distributed uniformly over the frontal cortex while and IBA1 immunoreactivity was clearly detectable in activated microglia around plaques. C4B staining was strongly visible in microglia forming an outer rim around the plaques. To quantify protein expression levels, we performed Western blot analysis of IBA1, GFAP, and C4B in the frontal cortex of APPswe/PS1dE9 mice (Fig. 3B). Quantification of the immunoblots revealed that GFAP and IBA1 protein expression significantly increased over time (ANOVA, $p < 0.05$). We observed a mild, but nonsignificant, increase of C4B protein expression (ANOVA, $p = 0.5$; $p = 0.28$ when an outlier was removed). Wild type animals did not show significant changes in protein expression of GFAP, IBA1, and C4B over time (data not shown).

### 3.5. Plaque formation is not associated with transcriptional alterations of genes involved in synaptic activity or plasticity

Changes in synaptic transmission and plasticity related genes occur early in AD patients in Braak stages 2 and 3 (Bossers et al., 2010a). However, in APPswe/PS1dE9 mice the analysis of differential gene expression and the GO analysis did not reveal transcriptional alterations in genes that have a function in synaptic activity or plasticity during Aβ plaque formation. To confirm that key synaptic genes were indeed not regulated in APPswe/PS1dE9 mice we performed an extensive qPCR analysis for the time points 2, 3, 6, 9, 12, and 15–18 months. The selection of synaptic genes was based on 2 criteria. First, 14 genes were selected that have been investigated in another very similar APP+PS1 mouse model for AD (Dickey et al., 2003; see Fig. 4 and Supplementary Table 1 for a specification of the studied genes and primer sequences). Seven of those genes were reported to be downregulated. Like the APPswe/PS1dE9 mouse, the APP+PS1 mouse carries the Swedish mutation of APP (K670N, M671L), but a different PS1 mutation (M146L) (Holcomb et al., 1998). Second, 9 genes were selected because these have been shown to be regulated in a recent microarray study in human postmortem prefrontal cortex tissue of AD patients (Bossers et al., 2010a). The qPCR analysis showed that only 3 well-studied synaptic genes—early growth response 1 (Egr1), activity regulated cytoskeletal-associated protein (Arc), and nuclear receptor subfamily 4, group A, member 1 (Nr4a1)—showed a trend

**Table 1**
List of significantly altered transcripts in APPswe/PS1dE9 transgenic mice during the development of beta amyloid protein (Aβ) pathology

| GeneName | Description | 2 Mo | 3 Mo | 6 Mo | 9 Mo | 12 Mo | 15–18 Mo | *p* | Fold change | Cluster |
|---|---|---|---|---|---|---|---|---|---|---|
| *Cst7* | Mus musculus cystatin F (leukocystatin) (Cst7), mRNA [NM_009977] | 0.4 | 0.44 | 3.78 | 5.58 | 6.93 | 7.17 | 2.29E−11 | 109.14 | 8 |
| *Itgax* | Mus musculus integrin alpha X (Itgax), mRNA [NM_021334] | 0.58 | 0.12 | 1.56 | 3.29 | 4.66 | 5.26 | 3.04E−06 | 35.26 | 8 |
| *Clec7a* | Mus musculus C-type lectin domain family 7, member a (Clec7a), mRNA [NM_020008] | −0.13 | −0.11 | 1.7 | 3.42 | 4.19 | 4.72 | 2.45E−06 | 28.84 | 8 |
| *Ccl3* | Mus musculus chemokine (C-C motif) ligand 3 (Ccl3), mRNA [NM_011337] | 0.17 | 0 | 2.14 | 3.65 | 4.38 | 4.59 | 2.47E−07 | 24.08 | 8 |
| *C4b* | Mus musculus complement component 4B (Childo blood group) (C4b), mRNA [NM_009780] | 0.36 | 0.27 | 1.8 | 2.79 | 3.9 | 4.54 | 3.74E−04 | 19.29 | 8 |
| *Ccl4* | Mus musculus chemokine (C-C motif) ligand 4 (Ccl4), mRNA [NM_013652] | −0.04 | −0.05 | 1.5 | 2.85 | 3.78 | 3.98 | 3.98E−09 | 16.34 | 8 |
| *Gpnmb* | Mus musculus glycoprotein (transmembrane) nmb (Gpnmb), mRNA [NM_053110] | 0.15 | 0.12 | 0.73 | 1.63 | 3 | 4.06 | 1.32E−05 | 15.35 | 8 |
| *Gpr109* | Mus musculus G protein-coupled receptor 109A (Gpr109a), mRNA [NM_030701] | 0.13 | −0.02 | 1.1 | 2.53 | 3.46 | 3.84 | 4.56E−08 | 14.52 | 8 |
| *Ccl6* | Mus musculus chemokine (C-C motif) ligand 6 (Ccl6), mRNA [NM_009139] | 0.09 | 0.25 | 1.71 | 3.04 | 3.84 | 3.83 | 2.77E−09 | 13.45 | 8 |
| *Pdcd1* | Mus musculus programmed cell death 1 (Pdcd1), mRNA [NM_008798] | 0.09 | 0.14 | 1.28 | 2.43 | 3.18 | 3.62 | 2.77E−06 | 11.55 | 8 |
| *Igf1* | Mus musculus insulin-like growth factor 1 (Igf1), mRNA [NM_010512] | 0.01 | −0.3 | 0.24 | 1.27 | 2.43 | 2.85 | 1.92E−11 | 8.88 | 8 |
| *Gfap* | Mus musculus glial fibrillary acidic protein (Gfap), mRNA [NM_010277] | 0.03 | 0 | 1.12 | 1.8 | 2.41 | 2.99 | 0.014 | 7.94 | 8 |
| *Trem2* | Mus musculus triggering receptor expressed on myeloid cells 2 (Trem2), mRNA [NM_031254] | 0.01 | 0.21 | 0.84 | 1.84 | 2.62 | 2.95 | 2.38E−06 | 7.67 | 8 |
| *Spp1* | Mus musculus secreted phosphoprotein 1 (Spp1), mRNA [NM_009263] | 0.09 | −0.17 | 0.13 | 0.71 | 1.68 | 2.74 | 3.16E−04 | 7.52 | 8 |
| *Bcl3* | Mus musculus B-cell leukemia/lymphoma 3 (Bcl3), mRNA [NM_033601] | 0.08 | −0.28 | 0.17 | 1.03 | 1.79 | 2.49 | 0.033 | 6.82 | 8 |
| *Bcl2a1b* | Mus musculus B-cell leukemia/lymphoma 2 related protein A1b (Bcl2a1b), mRNA [NM_007534] | −0.02 | −0.25 | 0.24 | 1.69 | 2.3 | 2.51 | 4.04E−04 | 6.77 | 8 |
| *Cd300lf* | Mus musculus CD300 antigen like family member F (Cd300lf), mRNA [NM_145634] | −0.03 | −0.15 | 0.82 | 2.1 | 2.4 | 2.45 | 1.22E−06 | 6.06 | 8 |
| *Tlr2* | Mus musculus toll-like receptor 2 (Tlr2), mRNA [NM_011905] | 0 | −0.1 | 0.74 | 1.71 | 2.34 | 2.49 | 0.001 | 6.02 | 8 |
| *Ch25h* | Mus musculus cholesterol 25-hydroxylase (Ch25h), mRNA [NM_009890] | 0.05 | −0.14 | 0.38 | 1.56 | 2.19 | 2.43 | 6.49E−05 | 5.94 | 8 |
| *Cd68* | Mus musculus CD68 antigen (Cd68), mRNA [NM_009853] | 0.23 | 0.14 | 0.81 | 1.57 | 2.42 | 2.63 | 0.022 | 5.62 | 8 |
| *Tyrobp* | Mus musculus TYRO protein tyrosine kinase binding protein (Tyrobp), mRNA [NM_011662] | −0.02 | 0.03 | 0.59 | 1.67 | 2.3 | 2.44 | 4.02E−06 | 5.50 | 8 |
| *Fcgr2b* | Mus musculus Fc receptor, IgG, low affinity IIb (Fcgr2b), mRNA [NM_001077189] | 0 | −0.23 | 0.29 | 1.26 | 2.06 | 2.22 | 6.13E−06 | 5.46 | 8 |
| *Lzp-s* | Mus musculus P lysozyme structural (Lzp-s), mRNA [NM_013590] | 0.22 | 0.25 | 0.53 | 2 | 2.49 | 2.66 | 0.005 | 5.43 | 8 |
| *St14* | Mus musculus suppression of tumorigenicity 14 (colon carcinoma) (St14), mRNA [NM_011176] | 0.15 | 0.15 | 0.82 | 1.56 | 2.33 | 2.58 | 0.008 | 5.39 | 8 |
| *Cd52* | Mus musculus CD52 antigen (Cd52), mRNA [NM_013706] | 0.23 | 0.2 | 1.06 | 2 | 2.6 | 2.62 | 9.33E−04 | 5.35 | 8 |
| *Cxcl5* | Mus musculus chemokine (C-X-C motif) ligand 5 (Cxcl5), mRNA [NM_009141] | −0.18 | −0.05 | 0.63 | 1.41 | 2.15 | 2.23 | 0.001 | 5.31 | 8 |
| *Gpr65* | Mus musculus G-protein coupled receptor 65 (Gpr65), mRNA [NM_008152] | −0.07 | −0.09 | 0.64 | 1.64 | 2.04 | 2.32 | 2.42E−09 | 5.31 | 8 |
| *Cd14* | Mus musculus CD14 antigen (Cd14), mRNA [NM_009841] A430060F13Rik Mus musculus 2 cells egg cDNA, RIKEN full-length enriched library, clone:B020003F03 product:hypothetical protein, full insert sequence. [AK139527] | 0.11 | 0.05 | 0.62 | 1.37 | 2.11 | 2.42 | 4.00E−03 | 5.17 | 8 |
| *Mamdc2* | Mus musculus MAM domain containing 2 (Mamdc2), mRNA [NM_174857] | 0.04 | 0.05 | −0.09 | 0.49 | 1.62 | 2.28 | 6.93E−09 | 5.17 | 8 |
| *4930431B09Rik* | Mus musculus cDNA clone IMAGE:6306854, partial cds. [BC046309] | 0.05 | 0.17 | 0.84 | 1.62 | 2.4 | 2.39 | 6.13E−06 | 5.10 | 8 |
| *Asb10* | Mus musculus ankyrin repeat and SOCS box-containing protein 10 (Asb10), Mrna [NM_080444] | 0 | −0.18 | 0.46 | 1.38 | 2 | 2.15 | 0.03 | 5.03 | 8 |
| *AU020206* | Mus musculus 7 days embryo whole body cDNA, RIKEN full-length enriched library, clone:C430005K08 product:unclassifiable, full insert sequence [AK049415] | 0 | 0.12 | 0.85 | 1.92 | 2.28 | 2.32 | 2.73E−07 | 4.99 | 8 |
| *Osmr* | Mus musculus oncostatin M receptor (Osmr), mRNA [NM_011019] | 0.01 | −0.15 | 0.18 | 0.96 | 1.41 | 2.14 | 1.39E−08 | 4.89 | 8 |
| *Ly86* | Mus musculus lymphocyte antigen 86 (Ly86), mRNA [NM_010745] | −0.08 | −0.03 | 0.6 | 1.55 | 2.08 | 2.2 | 4.70E−10 | 4.86 | 8 |
| *Cd84* | Mus musculus CD84 antigen (Cd84), mRNA [NM_013489] | −0.06 | −0.15 | 0.51 | 1.41 | 1.85 | 2.08 | 1.54E−06 | 4.69 | 8 |
| *Slc15a3* | Mus musculus solute carrier family 15, member 3 (Slc15a3), mRNA [NM_023044] | 0.07 | −0.21 | 0.5 | 1.21 | 1.95 | 2.01 | 0.026 | 4.66 | 8 |
| *Syngr1* | Mus musculus synaptogyrin 1 (Syngr1), transcript variant 1b, mRNA [NM_009303] | 0.08 | 0.1 | 0.53 | 1.34 | 2.11 | 2.3 | 0.003 | 4.66 | 8 |

**Table 1** (*continued*)

| GeneName | Description | 2 Mo | 3 Mo | 6 Mo | 9 Mo | 12 Mo | 15–18 Mo | *p* | Fold change | Cluster |
|---|---|---|---|---|---|---|---|---|---|---|
| *Slc11a1* | Mus musculus solute carrier family 11 (proton-coupled divalent metal ion transporters), member 1 (Slc11a1), mRNA [NM_013612] | 0.17 | 0.01 | 0.63 | 1.41 | 2.05 | 2.21 | 0.029 | 4.59 | 8 |
| *Siglecf* | Mus musculus sialic acid binding Ig-like lectin F (Siglecf), mRNA [NM_145581] | 0.03 | −0.18 | 0.52 | 1.54 | 1.9 | 1.94 | 6.49E−05 | 4.35 | 8 |
| *5430435G22Rik* | Mus musculus RIKEN cDNA 5430435G22 gene (5430435G22Rik), mRNA [NM_145509] | −0.05 | −0.48 | −0.03 | 0.6 | 1.34 | 1.56 | 9.60E−09 | 4.11 | 8 |
| *Irf8* | Mus musculus interferon regulatory factor 8 (Irf8), mRNA [NM_008320] | 0.15 | 0.08 | 0.64 | 1.34 | 1.93 | 2.08 | 0.011 | 4.00 | 8 |
| *Ctsz* | Mus musculus cathepsin Z (Ctsz), mRNA [NM_022325] | 0.13 | 0.21 | 0.83 | 1.44 | 1.94 | 2.04 | 0.009 | 3.76 | 8 |
| *Lrmp* | Mus musculus lymphoid-restricted membrane protein (Lrmp), mRNA [NM_008511] | 0.09 | 0.19 | 0.95 | 1.35 | 1.67 | 1.94 | 5.54E−05 | 3.61 | 8 |
| *Pon3* | Mus musculus paraoxonase 3 (Pon3), mRNA [NM_173006] | 0.02 | −0.14 | 0.32 | 0.98 | 1.54 | 1.7 | 0.004 | 3.58 | 8 |
| *Samsn1* | Mus musculus SAM domain, SH3 domain and nuclear localization signals, 1 (Samsn1), mRNA [NM_023380] | −0.05 | −0.21 | −0.21 | 0.9 | 1.29 | 1.61 | 0.002 | 3.53 | 8 |
| *Cd9* | Mus musculus CD9 antigen (Cd9), mRNA [NM_007657] | 0.13 | 0 | 0.57 | 1.12 | 1.61 | 1.78 | 1.13E−06 | 3.43 | 4 |
| *Ebi2* | Mus musculus Epstein-Barr virus induced gene 2 (Ebi2), mRNA [NM_183031] | −0.02 | −0.26 | 0.05 | 0.73 | 1.28 | 1.5 | 7.31E−04 | 3.39 | 8 |
| *Mpeg1* | PREDICTED: Mus musculus macrophage expressed gene 1, transcript variant 1 (Mpeg1), mRNA [XM_129176] | −0.09 | −0.25 | 0.24 | 1.06 | 1.49 | 1.5 | 6.02E−04 | 3.36 | 8 |
| *Atf3* | Mus musculus activating transcription factor 3 (Atf3), mRNA [NM_007498] | 0.1 | 0.13 | 0.64 | 1.21 | 1.75 | 1.84 | 0.036 | 3.34 | 8 |
| *Gusb* | Mus musculus glucuronidase, beta (Gusb), mRNA [NM_010368] | 0.08 | 0.17 | 0.59 | 1.27 | 1.79 | 1.71 | 2.59E−04 | 3.27 | 8 |
| *Cd300d* | Mus musculus Cd300D antigen (Cd300d), mRNA [NM_134158] | 0.04 | 0.01 | 0.29 | 1 | 1.52 | 1.71 | 7.00E−04 | 3.25 | 8 |
| *Birc1b* | Mus musculus baculoviral IAP repeat-containing 1b (Birc1b), mRNA [NM_010872] | 0.1 | −0.14 | 0.5 | 1.36 | 1.54 | 1.51 | 0.01 | 3.20 | 8 |
| *C1qc* | Mus musculus complement component 1, q subcomponent, C chain (C1qc), mRNA [NM_007574] | 0.11 | 0.06 | 0.48 | 0.99 | 1.52 | 1.72 | 0.032 | 3.16 | 4 |
| *Fcgr3* | Mus musculus Fc receptor, IgG, low affinity III (Fcgr3), mRNA [NM_010188] | 0.09 | −0.04 | 0.42 | 1.1 | 1.61 | 1.55 | 0.01 | 3.14 | 8 |
| *Lair1* | Mus musculus leukocyte-associated Ig-like receptor 1 (Lair1), mRNA [NM_178611] | −0.06 | 0.04 | 0.52 | 1.05 | 1.39 | 1.57 | 1.17E−04 | 3.10 | 4 |
| *Cybrd1* | Mus musculus adult male urinary bladder cDNA, RIKEN full-length enriched library, clone: 9530059N16 product:cytochrome b reductase 1, full insert sequence [AK162525] | 0.05 | −0.44 | −0.21 | 0.33 | 0.95 | 1.19 | 0.004 | 3.10 | 4 |
| *Lilrb4* | Mus musculus leukocyte immunoglobulin-like receptor, subfamily B, member 4 (Lilrb4), RNA [NM_013532] | 0.17 | 0.1 | 0.28 | 0.84 | 1.28 | 1.71 | 7.03E−05 | 3.05 | 4 |
| *Baiap2l2* | Mus musculus BAI1-associated protein 2-like 2 (Baiap2l2), mRNA [NM_177580] | 0.19 | 0.18 | 0.55 | 0.89 | 1.41 | 1.66 | 0.017 | 2.79 | 4 |
| *Slc14a1* | Mus musculus solute carrier family 14 (urea transporter), member 1 (Slc14a1), mRNA [NM_028122] | 0.14 | −0.01 | 0.29 | 0.76 | 1.26 | 1.46 | 2.62E−05 | 2.77 | 4 |
| *Fyb* | Mus musculus FYN binding protein (Fyb), mRNA [NM_011815] | −0.12 | 0.01 | 0.34 | 0.94 | 1.14 | 1.34 | 0.031 | 2.75 | 4 |
| *Msr2* | Mus musculus macrophage scavenger receptor 2 (Msr2), mRNA [NM_030707] | −0.01 | −0.08 | 0.39 | 0.87 | 1.36 | 1.37 | 0.017 | 2.73 | 4 |
| *Apoc4* | Mus musculus apolipoprotein C-IV (Apoc4), mRNA [NM_007385] | 0.01 | −0.15 | 0.13 | 0.35 | 0.82 | 1.3 | 6.28E−04 | 2.73 | 4 |
| *Hexb* | Mus musculus hexosaminidase B (Hexb), mRNA [NM_010422] | −0.03 | −0.05 | 0.36 | 0.96 | 1.25 | 1.4 | 7.73E−05 | 2.73 | 4 |
| *Tnfsf13b* | Mus musculus tumor necrosis factor (ligand) superfamily, member 13b (Tnfsf13b), mRNA [NM_033622] | 0.06 | 0.03 | 0.28 | 1.16 | 1.47 | 1.47 | 0.022 | 2.71 | 4 |
| *Apbb1ip* | Mus musculus amyloid beta (A4) precursor protein-binding, family B, member 1 interacting protein (Apbb1ip), mRNA [NM_019456] | −0.16 | 0 | 0.2 | 0.62 | 0.96 | 1.21 | 2.00E−02 | 2.58 | 4 |
| *Ctsh* | Mus musculus cathepsin H (Ctsh), mRNA [NM_007801] | 0.01 | −0.19 | 0.11 | 0.7 | 1.05 | 1.18 | 6.45E−04 | 2.58 | 4 |
| *Ctsc* | Mus musculus cathepsin C (Ctsc), mRNA [NM_009982] | −0.01 | −0.23 | 0.04 | 0.76 | 1.03 | 1.12 | 0.01 | 2.55 | 4 |
| *Afp* | Mus musculus alpha fetoprotein (Afp), mRNA [NM_007423] | -0.04 | −0.13 | 0.13 | 0.62 | 0.84 | 1.2 | 0.011 | 2.51 | 4 |
| *Cd48* | Mus musculus CD48 antigen (Cd48), mRNA [NM_007649] | 0.06 | 0.04 | 0.23 | 0.91 | 1.14 | 1.36 | 0.043 | 2.50 | 4 |
| *Klhl6* | Mus musculus kelch-like 6 (Drosophila) (Klhl6), mRNA [NM_183390] | −0.04 | 0.24 | 0.45 | 0.85 | 1.27 | 1.26 | 0.002 | 2.48 | 4 |
| *Cd86* | Mus musculus CD86 antigen (Cd86), mRNA [NM_019388] | −0.05 | −0.16 | 0.09 | 0.64 | 0.88 | 1.12 | 1.05E−04 | 2.43 | 4 |
| *Plxdc2* | Mus musculus plexin domain containing 2 (Plxdc2), mRNA [NM_026162] | −0.16 | −0.1 | 0.24 | 0.77 | 1.05 | 1.11 | 2.23E−05 | 2.41 | 4 |
| *Lpl* | Mus musculus lipoprotein lipase (Lpl), mRNA [NM_008509] | −0.06 | −0.15 | 0.17 | 0.64 | 0.99 | 1.08 | 0.004 | 2.35 | 4 |
| *Ptx3* | Mus musculus pentraxin related gene (Ptx3), mRNA [NM_008987] | 0.02 | −0.1 | −0.11 | 0.39 | 0.6 | 1.05 | 0.006 | 2.23 | 4 |
| *B2m* | Mus musculus beta-2 microglobulin (B2m), mRNA [NM_009735] | −0.08 | 0.04 | 0.22 | 0.79 | 1.04 | 1.07 | 0.008 | 2.22 | 4 |
| *Aif1* | Mus musculus allograft inflammatory factor 1 (Aif1, Iba1), mRNA [NM_019467] | 0.08 | −0.01 | 0.36 | 0.79 | 1.14 | 1.07 | 0.005 | 2.22 | 4 |
| *D14Ertd668e* | Mus musculus DNA segment, Chr 14, ERATO Doi 668, expressed (D14Ertd668e), mRNA [NM_199015] | −0.07 | −0.13 | 0.16 | 0.7 | 0.9 | 1.01 | 0.027 | 2.20 | 4 |
| *Hpse* | Mus musculus heparanase (Hpse), mRNA [NM_152803] | 0.09 | −0.19 | −0.13 | 0.31 | 0.61 | 0.95 | 0.018 | 2.20 | 4 |

**Table 1** (*continued*)

| GeneName | Description | 2 Mo | 3 Mo | 6 Mo | 9 Mo | 12 Mo | 15–18 Mo | *p* | Fold change | Cluster |
|---|---|---|---|---|---|---|---|---|---|---|
| *Frrs1* | Mus musculus ferric-chelate reductase 1 (Frrs1), mRNA [NM_009146] | −0.04 | −0.12 | −0.06 | 0.58 | 1 | 0.79 | 0.004 | 2.17 | 4 |
| *Rnase4* | Mus musculus ribonuclease, RNase A family 4 (Rnase4), transcript variant 1, mRNA [NM_021472] | 0.02 | −0.1 | 0.15 | 0.53 | 0.83 | 1.01 | 0.019 | 2.16 | 4 |
| *EG328314* | Mus musculus adult male corpora quadrigemina cDNA, RIKEN full-length enriched library, clone:B230311A21 product: unclassifiable, full insert sequence [AK045784] | −0.01 | −0.04 | 0.28 | 0.87 | 0.99 | 1.02 | 0.031 | 2.08 | 4 |
| *Cd180* | Mus musculus CD180 antigen (Cd180), mRNA [NM_008533] | 0.04 | −0.09 | 0.32 | 0.86 | 0.95 | 0.85 | 0.047 | 2.06 | 4 |
| *Btk* | Mus musculus Bruton agammaglobulinemia tyrosine kinase (Btk), mRNA [NM_013482] | 0.04 | −0.03 | 0.21 | 0.63 | 0.97 | 0.9 | 0.039 | 2.00 | 4 |
| *Arpc1b* | Mus musculus actin related protein 2/3 complex, subunit 1B (Arpc1b), mRNA [NM_023142] | 0.02 | −0.01 | 0.08 | 0.56 | 0.93 | 0.89 | 3.68E−05 | 1.92 | 4 |
| *Apobec1* | Mus musculus apolipoprotein B editing complex 1 (Apobec1), mRNA [NM_031159] | 0.01 | 0.01 | 0.02 | 0.56 | 0.79 | 0.94 | 0.049 | 1.91 | 4 |
| *Rnaset2* | Mus musculus ribonuclease T2 (Rnaset2), transcript variant 1, mRNA [NM_026611] | 0.09 | 0.02 | 0.31 | 0.52 | 0.81 | 0.91 | 2.64E−04 | 1.85 | 4 |
| *Cnn3* | Mus musculus calponin 3, acidic (Cnn3), mRNA [NM_028044] | 0.04 | 0.06 | 0.33 | 0.49 | 0.69 | 0.73 | 0.012 | 1.61 | 4 |

Age data are presented as $^2$log-transformed fold change against average of all 2-month-old animals (wild type and transgenic). *p* values are Benjamini–Hochberg corrected ANOVA values. Fold change = maximum fold change between age groups. Cluster = cluster assignment (see Figure 2). All genes with $p < 0.05$ are listed. Abbreviations: mRNA, messenger RNA; Mo, months.

(Egr1: $p = 0.09$; Arc: $p = 0.16$; Nr4a1 $p = 0.08$) toward decrease in aged transgenic APPswe/PS1dE9 mice (15–18 months) compared with age-matched wild type animals. These 3 genes were also reported to be downregulated in the study by Dickey and colleagues (2003). None of the other synaptic genes, including those that were found to be changed in the human data set, showed alterations in mRNA expression. Importantly, for all of the genes, the qPCR data corroborated the APPswe/PS1dE9 microarray results.

### 3.6. APPswe/PS1dE9 and human AD data show very limited overlap

To further investigate the similarities and differences between gene expression changes in the APPswe/PS1dE9 mouse and the human AD brain, we performed a qPCR study on 8 genes (Bcl2, Btg1, Cd59, Gtf2i, Mxi1, Slc6a12, Cycs, Chchd2) that we have found to be consistently regulated in at least 3 out of 5 published human AD microarray data sets (Blalock et al., 2004; Bossers et al., 2010a; Emilsson et al., 2006; Parachikova et al., 2007; Xu et al., 2006). None of these genes showed a significant regulation of expression in the APPswe/PS1dE9 mouse model at 2, 3, 6, 9, 12, and 15–18 months of age. However, the Bcl-2 like gene Bcl2a1b was significantly upregulated on the mouse microarray.

We also investigated whether transcriptional changes that occurred in APPswe/PS1dE9 mice with developing plaque pathology were comparable with gene expression changes in the human brain during the progression of sporadic AD (Bossers et al., 2010a). This data set contains gene expression data of the gray matter of the prefrontal cortex before and after plaque development and a comparison with the APPswe/PS1dE9 data set might thus elucidate whether transcriptional changes associated with Aβ plaque development in the mouse are similar to the human situation. The analysis of the overlap between the lists of significantly regulated genes in the APPswe/PS1dE9 data set ($n = 87$ genes) and the human data set ($n = 922$ genes) revealed that only 3 genes (solute carrier family 14 [urea transporter] member 1 [Slc14a1], C4b, plexin domain containing 2 [Plxdc2]) were significantly upregulated in both the mouse and human data sets with increasing plaque load or Braak stages, respectively.

A comparison of the overrepresented biological process GO classes in the 2 data sets also revealed a minimal overlap between mouse and human data. The mouse clusters were associated with immune response. In the human AD brain, however, the clusters of downregulated genes are associated with synaptic activity and plasticity and the clusters with upregulated genes are associated with transcription, metal ion binding, differentiation/proliferation and, as small overlap with the mouse data, antigen processing (Bossers et al., 2010a). Comparing only the immune response-related clusters in the APPswe/PS1dE9 mouse and sporadic AD data, we found that C3, C4B, CXCL10, CXCR4, histocompatibility complex, class II, DR β 1 (HLA-DRB1), ICOSLG, IRAK3, KLHL6, RGS1, Serpin peptidase inhibitor, clade A [alpha-1 antiproteinase, antitrypsin], member 3 [SERPINA3], TGFB1 and TREM2 were upregulated in both data sets.

## 4. Discussion

In the present study we used microarray technology to examine which transcriptional changes occur in the frontal cortex of the double-transgenic mouse line APPswe/PS1dE9 before, during, and after the development of dense-core Aβ plaques and to compare these transcriptional alterations to transcriptional changes in the human AD brain. Only a limited number of studies have explored genome-wide transcriptional changes at 2 or 3 time points during the development of Aβ plaques in AD mouse models: in the cerebral cortex (Reddy et al., 2004) of the Tg2576 ($APP695^{KM670/671NL}$), the $APP^{NLh/NLh}$/$PS\text{-}1^{P264L/P264L}$, the Tg2576/$PS^{P264L/P264L}$, and the Tg2576/$PS^{P264L/+}$ mouse (Wu et al., 2006), and the hippocampus and cortex of the PDAPP ($APP^{V717}$) mouse (Selwood et al., 2009). The results from these experiments were remarkably diverse and included the upregulation of apoptotic genes (Reddy et al., 2004), the upregulation of genes involved in mitochondrial energy metabolism (Reddy et al., 2004), the upregulation of carbohydrate metabolism and proteolysis (Wu et al., 2006), the downregulation of transcription and translation (Selwood et al., 2009), the upregulation of immune response related genes (Wu et al., 2006) and the downregulation of genes involved in neuronal survival (Selwood et al., 2009; Wu et al., 2006). These studies investigated genome-wide patterns of gene expression at 2 or 3 time points throughout the progression of Aβ pathology. However, they focused only on either intermediate stages (Selwood et al., 2009), or early and late stages (Reddy et al., 2004; Wu et al., 2006) of the plaque pathology. In the current study we investigated the whole time profile from 2 to 18 months to monitor closely the transcriptional changes that occur before and during the buildup of Aβ pathology.

To follow the expression of individual transcripts during the development of Aβ plaque pathology, we constructed expression profiles over time. This approach revealed 2 clusters of concerted

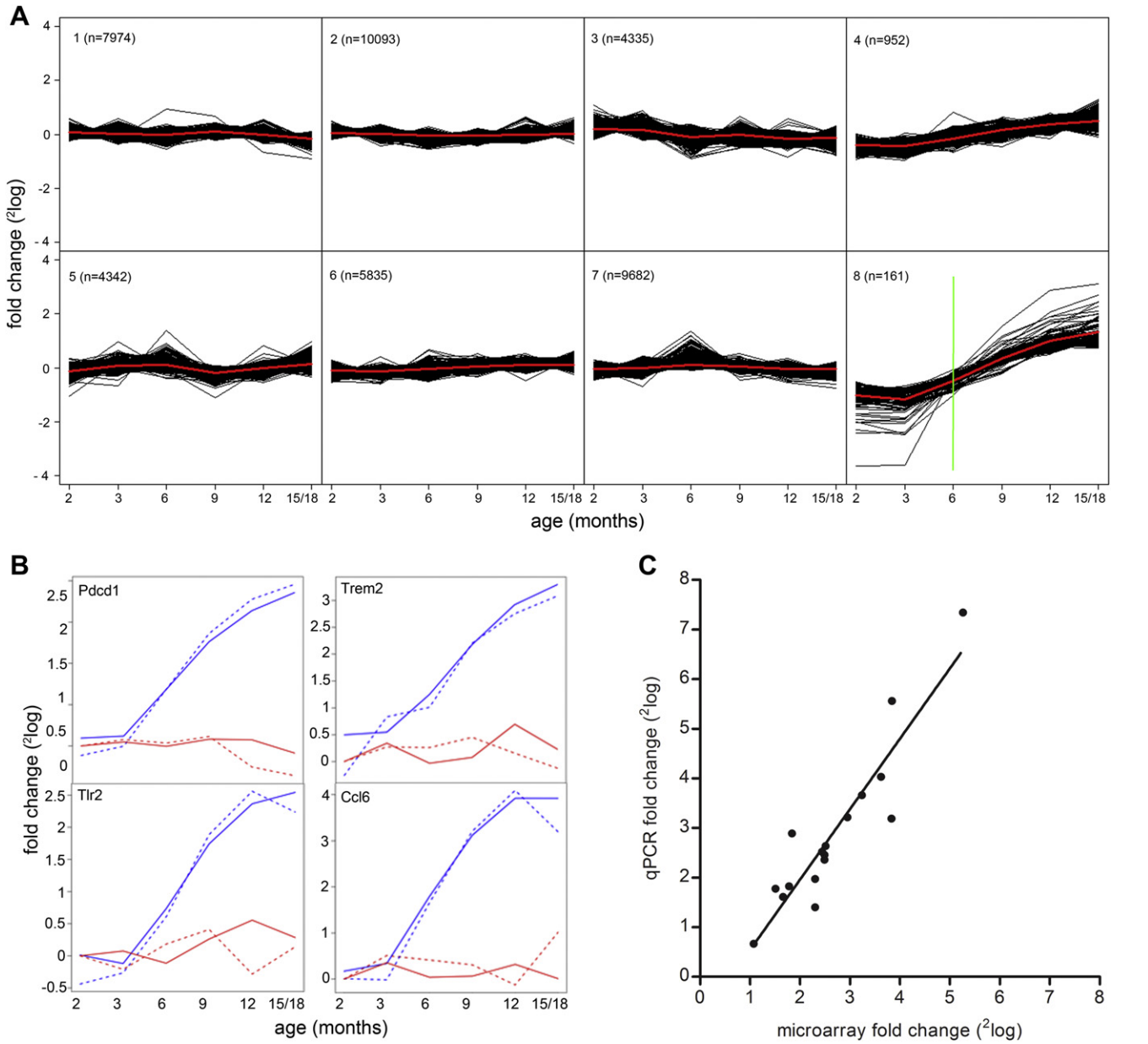


**Fig. 2.** Upregulation of gene transcripts during the development of beta amyloid protein (Aβ) pathology in APPswe/PS1dE9 mice. (A) Genes were clustered according to their expression profiles over time in APPswe/PS1dE9 transgenic mice. Expression values were normalized against the mean expression of all 2-month-old animals. Cluster 4 contains 3.9% and cluster 8 contains 67% significantly regulated genes. The red solid line indicates the average expression profile of all cluster members. The green solid line indicates the first time point when we detected Aβ pathology in the mice. Note that gene upregulation coincided with the buildup of pathology and that no downregulated genes were detected. (B) Example profiles of quantitative polymerase chain reaction (qPCR) validations for programmed cell death 1 (Pdcd1), triggering receptor expressed on myeloid cells 2 (Trem2), toll-like receptor 2 (Tlr2), and chemokine ligand 6 (Ccl6). The microarray data (solid lines) correlated with the qPCR data (dashed lines) for wild type (red) and transgenic (blue) animals over time. (C) The scatter plot shows correlation data between qPCR and microarray for 17 genes in 15–18-month-old APPswe/PS1dE9 transgenic mice ($R^2 = 0.85$, $p < 0.001$).

upregulated genes over the progression of plaque pathology with pronounced transcriptional changes detected from the age of 6 months onward, suggesting a link between the development of plaque pathology and transcription of these genes. However, because we have not investigated time points in between 3 and 6 months, we cannot further specify whether gene upregulation starts shortly before, shortly after, or at the same time as the appearance of the first plaques.

### *4.1. Plaque development in APPswe/PS1dE9 mice is accompanied by astroglial and microglial activation*

We compared the significantly regulated genes of our data set with transcriptome databases for genes enriched in astrocytes, oligodendrocytes, neurons (Cahoy et al., 2008), and microglia (Thomas et al., 2006) to investigate whether those genes, whose expression is induced at the time that Aβ pathology becomes apparent in the cortex of the APPswe/PS1dE9, are expressed in a particular cell type. The great majority of significantly regulated genes were expressed in microglia (53 genes: Afp, Aif1, Apbb1ip, Apobec1, Arpc1b, Asb10, Atf3, B2m, Bcl3, Birc1b, Btk, Ccl3, Ccl4, Ccl6, Cd14, Cd48, Cd52, Cd68, Cd84, Cd86, Cd9, Cst7, Ctsc, Ctsh, Ctsz, Ebi2, Fcgr2b, Fcgr3, Gpnmb, Gpr65, Gusb, Igf1, Itgax, Klhl6, Lair1, Lilrb4, Lpl, Lrmp, Ly86, Mamdc2, Mpeg1, Pon3, Rnase4, Rnaset2, Samsn1, Slc11a1, Slc15a3, Spp1, Syngr1, Tlr2, Tnfsf13b, Trem2, Tyrobp). Twenty of the significantly regulated genes (Atf3, AU020206, B2m, Bcl2a1b, C4b, Cd14, Cnn3, Ctsc Ctsz, Cybrd1, Frrs1, Gfap, Gusb,

**Table 2**
Table of the 30 most significantly regulated Gene Ontology (GO) identifiers in clusters 4 and 8

| ID | Term | Cluster number | Annotated | In cluster | *p* |
|---|---|---|---|---|---|
| Biological process | | | | | |
| GO:0002376 | Immune system process | 4 | 576 | 102 | 1.61E−74 |
| GO:0006955 | Immune response | 4 | 354 | 72 | 3.33E−63 |
| GO:0006952 | Defense response | 4 | 371 | 54 | 9.13E−28 |
| GO:0009605 | Response to external stimulus | 4 | 389 | 47 | 4.27E−17 |
| GO:0019882 | Antigen processing and presentation | 4 | 46 | 21 | 3.02E-16 |
| GO:0045321 | Leukocyte activation | 4 | 191 | 29 | 2.93E−15 |
| GO:0001775 | Cell activation | 4 | 204 | 30 | 4.62E−15 |
| GO:0048002 | antigen processing and Presentation of peptide antigen | 4 | 29 | 16 | 4.72E−14 |
| GO:0006954 | Inflammatory response | 4 | 179 | 27 | 4.72E−14 |
| GO:0006952 | Defense response | 8 | 371 | 21 | 6.23E−14 |
| GO:0009611 | Response to wounding | 4 | 251 | 33 | 7.31E−14 |
| GO:0006955 | Immune response | 8 | 354 | 20 | 2.00E-13 |
| GO:0046649 | Lymphocyte activation | 4 | 175 | 26 | 3.22E-13 |
| GO:0030097 | Hemopoiesis | 4 | 194 | 27 | 2.29E−12 |
| GO:0002520 | Immune system development | 4 | 231 | 30 | 2.62E−12 |
| GO:0002376 | Immune system process | 8 | 576 | 22 | 1.20E−11 |
| GO:0048534 | Hemopoietic or lymphoid organ development | 4 | 217 | 28 | 2.79E−11 |
| GO:0006954 | Inflammatory response | 8 | 179 | 14 | 5.05E−11 |
| GO:0009611 | Response to wounding | 8 | 251 | 14 | 4.05E−09 |
| GO:0051239 | Regulation of multicellular organismal process | 4 | 251 | 28 | 1.46E−08 |
| GO:0002478 | antigen processing and Presentation of exogenous peptide antigen | 8 | 17 | 6 | 2.25E−08 |
| GO:0002449 | Lymphocyte-mediated immunity | 8 | 78 | 9 | 2.25E−08 |
| GO:0006911 | Phagocytosis, engulfment | 8 | 9 | 5 | 2.97E−08 |
| GO:0002443 | Leukocyte-mediated immunity | 8 | 84 | 9 | 2.97E−08 |
| GO:0002474 | Antigen processing and presentation of peptide antigen via MHC class I | 4 | 15 | 9 | 3.58E−08 |
| GO:0051707 | Response to other organism | 8 | 124 | 10 | 4.33E−08 |
| GO:0050764 | Regulation of phagocytosis | 8 | 10 | 5 | 4.34E−08 |
| GO:0050766 | Positive regulation of phagocytosis | 8 | 10 | 5 | 4.34E−08 |
| GO:0009605 | Response to external stimulus | 8 | 389 | 15 | 4.34E−08 |
| GO:0002252 | Immune effector process | 4 | 115 | 21 | 5.13E−08 |
| Cellular component | | | | | |
| GO:0009986 | Cell surface | 4 | 163 | 27 | 3.21E−16 |
| GO:0042611 | MHC protein complex | 4 | 20 | 13 | 1.24E−12 |
| GO:0005886 | Plasma membrane | 4 | 1568 | 104 | 4.78E−10 |
| GO:0000323 | Lytic vacuole | 4 | 158 | 22 | 6.20E−10 |
| GO:0005764 | Lysosome | 4 | 158 | 22 | 6.20E−10 |
| GO:0009897 | External side of plasma membrane | 8 | 116 | 10 | 2.97E−08 |
| GO:0005773 | Vacuole | 4 | 177 | 22 | 4.27E−08 |
| GO:0009897 | External side of plasma membrane | 4 | 116 | 21 | 5.81E−08 |
| GO:0042612 | MHC class I protein complex | 4 | 12 | 8 | 9.12E−08 |
| GO:0009986 | Cell surface | 8 | 163 | 10 | 2.62E−07 |
| GO:0005764 | Lysosome | 8 | 158 | 9 | 1.72E−06 |
| GO:0000323 | Lytic vacuole | 8 | 158 | 9 | 1.72E−06 |
| GO:0005773 | Vacuole | 8 | 177 | 9 | 3.65E−06 |
| GO:0005886 | Plasma membrane | 8 | 1568 | 21 | 1.68E−05 |
| GO:0005576 | Extracellular region | 8 | 2041 | 24 | 6.18E−05 |
| GO:0016020 | Membrane | 4 | 6289 | 276 | 7.24E−05 |
| GO:0044421 | Extracellular region part | 4 | 1938 | 105 | 7.24E−05 |
| GO:0005615 | Extracellular space | 4 | 1828 | 100 | 8.17E−05 |
| GO:0042613 | MHC class II protein complex | 4 | 8 | 5 | 9.53E−05 |
| GO:0044459 | Plasma membrane part | 4 | 1216 | 72 | 1.24E−04 |
| GO:0044421 | Extracellular region part | 8 | 1938 | 22 | 3.24E−04 |
| GO:0005615 | Extracellular space | 8 | 1828 | 21 | 4.06E−04 |
| GO:0044459 | Plasma membrane part | 8 | 1216 | 16 | 4.40E−04 |
| GO:0016021 | Integral to membrane | 8 | 4812 | 39 | 2.12E−03 |
| GO:0031224 | Intrinsic to membrane | 8 | 4824 | 39 | 2.23E−03 |
| GO:0044425 | Membrane part | 4 | 5265 | 225 | 6.82E−03 |
| GO:0016021 | Integral to membrane | 4 | 4812 | 208 | 7.08E−03 |
| GO:0044425 | Membrane part | 8 | 5265 | 40 | 7.16E−03 |
| GO:0031224 | Intrinsic to membrane | 4 | 4824 | 208 | 7.98E−03 |
| Molecular function | | | | | |
| GO:0019865 | Immunoglobulin binding | 8 | 9 | 5 | 2.97E−08 |
| GO:0032403 | Protein complex binding | 8 | 43 | 6 | 1.43E−06 |
| GO:0019955 | Cytokine binding | 4 | 62 | 14 | 1.53E−06 |
| GO:0008009 | Chemokine activity | 8 | 34 | 5 | 8.18E−06 |
| GO:0042379 | Chemokine receptor binding | 8 | 35 | 5 | 9.16E−06 |
| GO:0001664 | G-protein-coupled receptor binding | 8 | 48 | 5 | 3.89E−05 |
| GO:0004896 | Cytokine receptor activity | 4 | 52 | 10 | 3.49E−04 |
| GO:0005515 | Protein binding | 4 | 4413 | 200 | 6.72E−04 |
| GO:0001784 | Phosphotyrosine binding | 8 | 6 | 2 | 2.27E−03 |
| GO:0003796 | Lysozyme activity | 8 | 7 | 2 | 3.10E−03 |

**Table 2** (*continued*)

| ID | Term | Cluster number | Annotated | In cluster | *p* |
|---|---|---|---|---|---|
| GO:0005125 | Cytokine activity | 4 | 196 | 17 | 3.68E−03 |
| GO:0005515 | Protein binding | 8 | 4413 | 36 | 3.75E−03 |
| GO:0045309 | Protein phosphorylated amino acid binding | 8 | 8 | 2 | 3.99E−03 |
| GO:0005509 | Calcium ion binding | 4 | 704 | 43 | 4.28E−03 |
| GO:0005102 | Receptor binding | 8 | 527 | 9 | 6.37E−03 |
| GO:0051219 | Phosphoprotein binding | 8 | 13 | 2 | 9.33E−03 |

Lair1, Mamdc2, Osmr, Plxdc2, Ptx3, Rnaset2, Slc14a1) were at least 1.5-fold enriched in astrocytes, with 3 (Cybrd1, Gfap, Slc14a1) being astrocyte-specific. It should be noted, however, that we found C4B protein expression in microglia and not in astrocytes. Only 4 significant genes were enriched in neurons (Ccl4, Igf1, Lpl, Syngr1). None of the regulated genes was enriched in oligodendrocytes.

The upregulation of many microglia genes including Cd68, a marker for activated microglia, indicates an activation of microglia by Aβ. This is in line with other studies reporting that IBA1 positive microglia express CD68 in AD mouse models (Bornemann et al., 2001; Kamphuis et al., 2012). Activated microglia are an effective response for the elimination of pathogens and are thought to mediate the degradation and clearance of Aβ (Boissonneault et al., 2009; Chen et al., 2006). Furthermore, the upregulation of many genes expressed in astrocytes indicates a clear involvement of astrocytes in Aβ pathology. Indeed, astrocytes are able to degrade Aβ (Wyss-Coray et al., 2003) and play an important role in the induction of neuroinflammation in AD (Li et al., 2011). Overall, our findings support earlier reports that astroglia become hypertrophic and that microglia tend to accumulate in and around senile plaques, both in animal models and in AD patients (Johnston et al., 2011; Kamphuis et al., 2012; Olabarria et al., 2010) and that they exhibit an activated phenotype (Yan et al., 2009) leading to the activation of host defense mechanisms.

### 4.2. APPswe/PS1dE9 mice exhibit a well-controlled immune response

Glial activation leads to the production of pro- and anti-inflammatory cytokines (Hanisch and Kettenmann, 2007; Li et al., 2011). Indeed, the great majority of upregulated transcripts in the APPswe/PS1dE9 mouse was involved in immune system related processes, including many Cd antigens, chemokine ligands, and members of the complement system. In contrast to earlier reports (Hickman et al., 2008; Ruan et al., 2009), our data show that in APPswe/PS1dE9 mice well-known proinflammatory mediators (Il-1, Il-6, tumor necrosis factor α [Tnfα], interferon γ, and Tgfß) were not significantly increased. Instead, we observed a strong upregulation of immune suppressive mediators like polypeptide growth factor 1 (Igf1) and triggering receptor expressed on myeloid cells 2 (Trem2). The production of proinflammatory cytokines such as Tnfα might be suppressed by the upregulation of Fc receptor gamma 2b (Fcgr2b) (Smith and Clatworthy, 2010), Igf1 (Gasparini

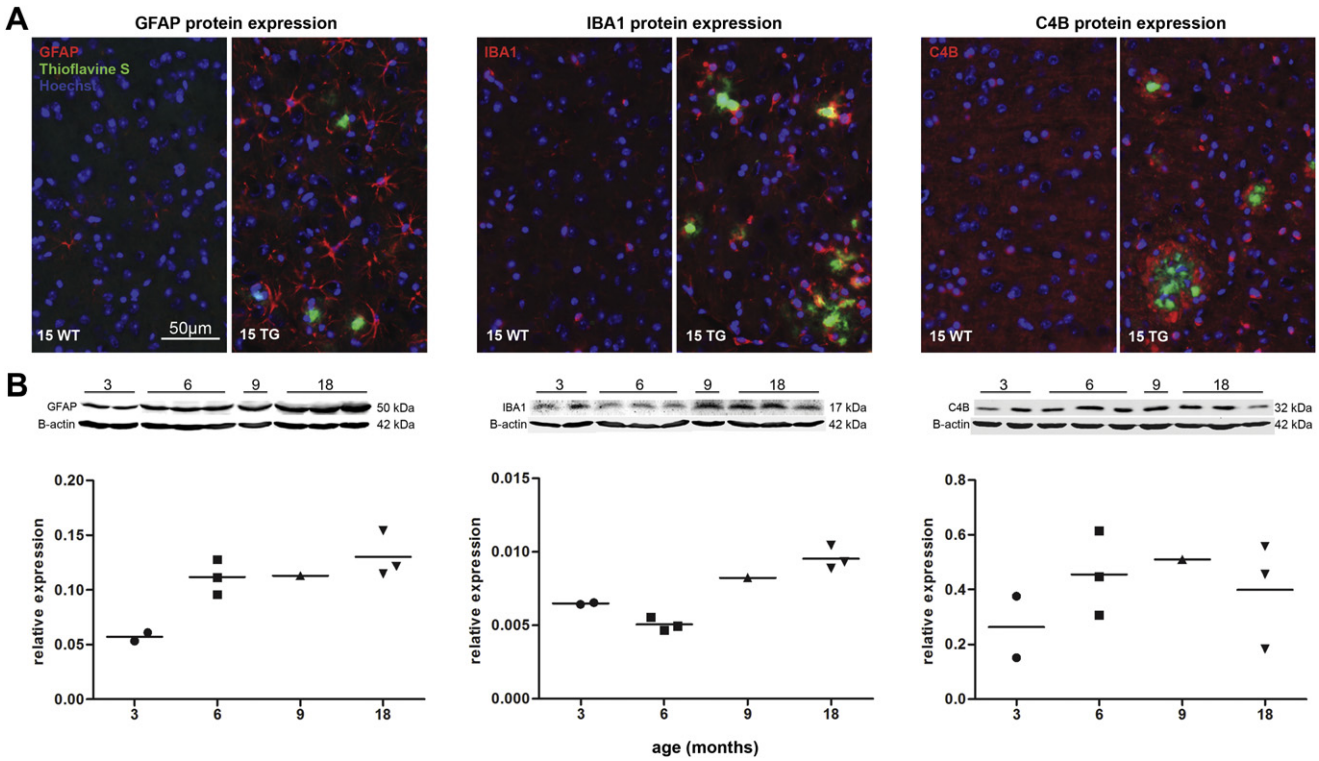


**Fig. 3.** Protein expression of glial-fibrillary acidic protein (GFAP), allograft inflammatory factor 1 (IBA1), and complement component 4b (C4B) in APPswe/PS1dE9 mice. (A) Fluorescent immunostaining on wild type (WT) and APPswe/PS1dE9 (TG) animals at 15 months. GFAP, IBA1, and C4B are shown in red; plaques were stained with thioflavine S and are shown in green; nuclei were stained with Hoechst and shown in blue. GFAP, IBA1, and C4B protein were upregulated in TG animals. Scale bar: 50 µm. (B) Western blot analysis and quantification for GFAP, IBA1, and C4B protein during the development of plaque pathology. Protein levels are given as relative values to β-actin levels. Western blot data for GFAP, IBA1, and C4B validated the microarray and the immunostainings even though the upregulation was less pronounced.

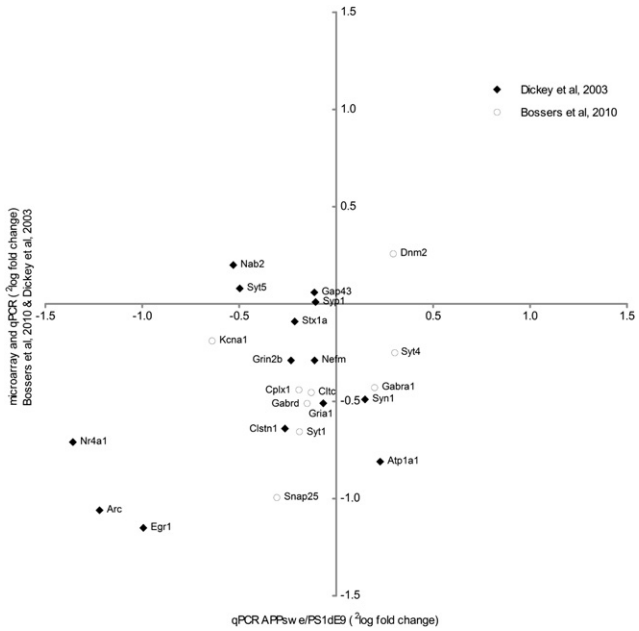


**Fig. 4.** Comparison of synaptic gene expression data from APPswe/PS1dE9 mice and literature. Gene expression of well-known synaptic genes that were investigated in another, but similar APP-PS1 transgenic mouse model (Dickey et al., 2003) or found to be regulated in human AD patients (Bossers et al., 2010a) was studied in APPswe/PS1dE9 mice using quantitative polymerase chain reaction (qPCR). Note that only Nr4a1, Arc, and Egr1 are mildly downregulated (not significant).

and Xu, 2003), Trem2 (Frank et al., 2008; Melchior et al., 2010), and programmed cell death 1 (Pdcd1) (Yao et al., 2009), molecules that have been indicated to decrease the severity of (auto)immune responses and to promote neuroprotective immune responses. As Tnfα, together with interferon γ, also stimulates Aβ deposition by inducing the production of Aβ peptides and decreasing the secretion of soluble APPs (Blasko et al., 1999), the successful reduction of Tnfα is, therefore, a frequently investigated therapeutic strategy for AD patients (Frankola et al., 2011; Park and Bowers, 2010). The APPswe/PS1dE9 mouse with its naturally occurring inhibition of Tnfα upregulation could possibly help to understand better which genes contribute to low Tnfα levels.

Furthermore, our data suggest that the upregulation of Atf3 in APPswe/PS1dE9 mice might serve as a control mechanism to limit the amount of Ccl4 (Khuu et al., 2007) and to inhibit Tlr2-stimulated inflammatory responses (Gilchrist et al., 2006; Liu et al., 2012; Sabroe et al., 2005). An excessive immune response might also be prevented by the upregulation of interferon regulatory factor 8 (Irf8) which negatively regulates MHC Class I molecules (Agrawal and Kishore, 2000). In general, our data suggest that Aβ invokes a well-controlled immune response to buildup rather than a strong inflammatory response in APPswe/PS1dE9 mice.

### 4.3. The expression of genes involved in synaptic function and plasticity is not altered in APPswe/PS1dE9 mice cortex

In our microarray and qPCR studies, we did not observe any significant transcriptional changes of genes with synaptic function in the APPswe/PS1dE9 mice. We observed only a single significantly upregulated gene, Syngr1, with reported synaptic function. Syngr1 is essential for short- and long-term potentiation in the hippocampus (Janz et al., 1999) and it inhibits $Ca^{2+}$-dependent exocytosis (Sugita et al., 1999). Syngr1 is localized to the membrane of small presynaptic vesicles (Kedra et al., 1998) and facilitates the targeting of synaptophysin to synaptic-like microvesicles in PC12 cells (Belfort and Kandror, 2003), a model system for synaptic vesicles. However, a study in human postmortem tissue showed that Syngr1 is down- and not upregulated in late onset AD patients (Liang et al., 2010).

Igf1 and Tlr2 are both strongly upregulated in the APPswe/PS1dE9 mice. In addition to their role in the immune system they have been implicated in neuronal functioning. Igf1 has neuroprotective effects and promotes neurogenesis, development, differentiation, synapse formation, and glucose utilization throughout the brain (Torres-Aleman, 2000). Furthermore, Igfl enhances cognitive performance, increases the levels of synaptic proteins (Carro et al., 2006), and reverses Aβ-induced neurotoxicity (Jarvis et al., 2007). In humans, IGF1 plasma levels are reduced in familial AD patients (Mustafa et al., 1999) and in aged subjects (Arvat et al., 2000). Tlr2 is involved in adult neurogenesis (Rolls et al., 2007). APP-PS1-Tlr2(-/-) mice show accelerated cognitive impairments paired with increased Aβ levels and Tlr2 treatment in these mice had beneficial effects by restoring the memory consolidation process (Richard et al., 2008). In humans, a polymorphism in Tlr2 changes the susceptibility to AD in a Chinese population (Yu et al., 2011). It is possible that the upregulation of Igf1 and Tlr2 helps to prevent neuronal damage in the frontal cortex of APPswe/PS1dE9 mice.

It has been suggested that amyloid might suppress molecular mechanisms for memory, independent of neuron or synapse loss (Dickey et al., 2003, 2004). However, Egr1, Arc, and Nr4a1, 3 immediate-early genes associated with long-term potentiation and memory consolidation, were the only genes associated with memory that showed a nonsignificant, decrease in the cortex of aged APPswe/PS1dE9 mice. This decrease was comparable with the decrease in the cortex and hippocampus of another APP+PS1 mouse model reported by Dickey and colleagues.

It is noteworthy that some studies show cognitive deficits in APPswe/PS1dE9 mice as early as 2–3 months (Pillay et al., 2008), 4 months (Bonardi et al., 2011), and 5 months (Timmer et al., 2010) of age. A larger body of evidence shows cognitive deficits at 6 months (Filali and Lalonde, 2009; Jankowsky et al., 2005; Kilgore et al., 2010; Lagadec et al., 2012; Minkeviciene et al., 2008) with the exception of a single study that could not detect cognitive deficits at that time point (Savonenko et al., 2005). Other studies have only investigated later time points and have consistently found cognitive deficits in older APPswe/PS1dE9 mice (Gimbel et al., 2010; Hooijmans et al., 2009; Melnikova et al., 2006; O'Leary and Brown, 2009; Toledo and Inestrosa, 2010). Most relevant to the cortical gene expression data presented here, Filali and Lalonde (2009) demonstrated that 6-month-old APPswe/PS1dE9 mice show deficits in nest building, which is indicative for prefrontal cortex dependent step-by-step planning and organization. Our transcriptional profiling data suggest that frontal cortex-dependent cognitive deficits in APPswe/PS1dE9 mice are not because of transcriptional changes of genes involved in learning and memory in cortical neurons. Because behavioral alterations can be caused by neuroinflammation (Arnaud et al., 2006; Fan et al., 2007; Labrousse et al., 2012; Zhang et al., 2012), the robust cognitive deficits in the APPswe/PS1dE9 mice starting at 6 months might partly be the result of changes in the expression of genes that govern an immune reaction. It should be noted that gene expression changes in other brain areas, such as the hippocampus, are very likely to contribute to frontal cortex-independent behavioral deficits.

### 4.4. APPswe/PS1dE9 mice transcriptional profiles do not resemble human AD data

In the present study we compared transcriptional changes in the frontal cortex of APPswe/PS1dE9 mice and AD patients during the development of AD pathology. In the human sporadic AD brain we observed that the appearance of AD neuropathology in Braak stage

3 is preceded by transcriptional changes in genes related to neuronal plasticity and activity in Braak stage 2 (Bossers et al., 2010a). We have not observed any evidence for changes in genes involved in these processes in the APPswe/PS1dE9 mouse. When comparing gene expression changes in end-stage AD patients (Braak stages 5 and 6) and aged APPswe/PS1dE9 mice, only 3 genes (Plxdc2, Slc14a1, and C4b) showed a significant regulation in both the transgenic APPswe/PS1dE9 mice and the sporadic human AD data sets. Blood-group antigen Slc14a1, an erythrocyte urea transporter, has so far no clear function in the nervous system (Bagnasco, 2006). Plxdc2 has been shown to coordinate cell proliferation and differentiation in the developing nervous system (Miller-Delaney et al., 2011) and in cancer (Carson-Walter et al., 2001; Davies et al., 2004; Rmali et al., 2007). Our finding that both genes are upregulated in an AD mouse model and in patients with Aβ plaques might suggest a yet unknown function for these genes in Aβ pathology. C4b, which is part of the classic activation pathway of the complement system, has been described to be highly expressed in and around plaques of the Arctic, Tg2576 (Fonseca et al., 2011) and APP+PS1 (Dickey et al., 2003) mouse models for AD and to prevent early stages of autoimmune disease (Paul et al., 2002). These results, together with our findings, suggest that C4b plays a role in Aβ-induced immune response.

In addition, we investigated whether genes that are consistently altered in multiple human AD microarray datasets (BCL2, BTG1, CD59, GTF2I, MXI1, SLC6A12, CYCS, and CHCHD2) (Blalock et al., 2004; Bossers et al., 2010a; Emilsson et al., 2006; Parachikova et al., 2007; Xu et al., 2006) are also altered in the APPswe/PS1dE9 mouse. We found that none of these genes are significantly altered in the cortex of APPswe/PS1dE9 mice. It should be noted that APPswe/PS1dE9 mice carry mutations in the APP and the PSEN1 gene, though these genes are not mutated in sporadic AD patients. The molecular mechanisms leading to plaque formation and memory deficits in these mice and sporadic AD patients might therefore be substantially different.

Functional annotations of regulated gene clusters in the transgenic mouse model hardly overlap with human data (Bossers et al., 2010a). Though the mouse only shows alterations in immune-related genes, the development and progression of AD in the human prefrontal cortex is associated with many (early) changes regarding synaptic activity, plasticity, transcription, metal ion binding, differentiation, and proliferation. The APPswe/PS1dE9 mouse is therefore not suitable for studying these aspects of AD, especially early synaptic changes.

### *4.5. The APPswe/PS1dE9 mouse can be a model for AD-related immune response*

Because we predominantly detected alterations in immune-related transcripts in APPswe/PS1dE9 mice, we specifically investigated whether we could find commonalities between human AD and the APPswe/PS1dE9 mouse in the regulation of immune-related transcripts other than the previously discussed genes TREM2 and C4B. Indeed, C3, CXCL10, CXCR4, HLA-DRB1, ICOSLG, IRAK3, KLHL6, RGS1, SERPINA3, and TGFB1 showed a trend toward upregulation in the cortex of the APPswe/PS1dE9 and the human AD data sets. Interestingly, most of these genes have been implicated in AD or amyloid pathology. Upregulation of the complement component C3 has been proposed to reduce Aβ plaque burden and neuronal loss by modulating microglia toward a classic M1-like activated phenotype (Maier et al., 2008) and activates Cd68. C3 upregulation itself is a result of anti-inflammatory Tgfb1 upregulation (Wyss-Coray et al., 2002). Tgfb1 also upregulates Irak3, a negative regulator of Toll-like receptor signaling (Standiford et al., 2011). The chemokine ligand CXCL10 is increased in brains of AD mouse models (Duan et al., 2008; Israelsson et al., 2010) and in cerebrospinal fluid of patients with mild AD (Galimberti et al., 2006), and chemokine receptor CXCR4 is downregulated in the Tg2576 mouse model for AD, but upregulated in AD patients (Parachikova and Cotman, 2007). The major HLA-DRB1 is expressed in antigen presenting dendritic cells and HLA-DR alleles might account for differences in Aβ-reactive T cells and Aβ immunogenicity (Zota et al., 2009). Polymorphisms in SERPINA3 have been implicated to modify the risk for AD associated with the apolipoprotein E ε4 allele (DeKosky et al., 1996; Kamboh et al., 1995, 2006).

Inflammation is a key contributing factor in the pathology of AD and many hallmarks of neuroinflammation (such as activation of microglia and the complement system, increased cytokine expression) are observed in tissue of AD patients (Eikelenboom et al., 2010, 2011; Frank-Cannon et al., 2009). Studying the immune response in AD is therefore essential for understanding the disease and developing therapies. Our study in the APPswe/PS1dE9 mouse model has uncovered the full temporal profile of transcriptional changes in immune genes that are associated with Aβ pathology, and provides a valuable resource to further elucidate the Aβ-induced immune response in AD.

## Disclosure statement

The authors declare no actual or potential conflict of interest.

All animal experiments were approved by the ethical committee for animal care and use of experimental animals of the Royal Netherlands Academy for Arts and Sciences, acting in accordance with the European Community Council directive of November 24, 1986 (86/609/EEC).

## Acknowledgements

We thank Inge Huitinga for her valuable suggestions during the preparation of the report. This work has been supported by the Top Institute Pharma (T5-207).

## Appendix A. Supplementary data

Supplementary data associated with this article can be found, in the online version, at http://dx.doi.org/10.1016/j.neurobiolaging.2012.11.008.

## References

Agrawal, S., Kishore, M.C., 2000. MHC class I gene expression and regulation. J. Hematother. Stem Cell Res. 9, 795–812.

Arnaud, L., Robakis, N.K., Figueiredo-Pereira, M.E., 2006. It may take inflammation, phosphorylation and ubiquitination to "tangle" in Alzheimer's disease. Neurodegener. Dis. 3, 313–319.

Arvat, E., Broglio, F., Ghigo, E., 2000. Insulin-Like growth factor I: implications in aging. Drugs Aging 16, 29–40.

Bagnasco, S.M., 2006. The erythrocyte urea transporter UT-B. J. Membr. Biol. 212, 133–138.

Beißbarth, T., Speed, T.P., 2004. GOstat: find statistically overrepresented Gene Ontologies within a group of genes. Bioinformatics 20, 1464–1465.

Belfort, G.M., Kandror, K.V., 2003. Cellugyrin and synaptogyrin facilitate targeting of synaptophysin to a ubiquitous synaptic vesicle-sized compartment in PC12 cells. J. Biol. Chem. 278, 47971–47978.

Bertram, L., Tanzi, R.E., 2005. The genetic epidemiology of neurodegenerative disease. J. Clin. Invest. 115, 1449–1457.

Blalock, E.M., Geddes, J.W., Chen, K.C., Porter, N.M., Markesbery, W.R., Landfield, P.W., 2004. Incipient Alzheimer's disease: microarray correlation analyses reveal major transcriptional and tumor suppressor responses. Proc. Natl. Acad. Sci. U. S. A 101, 2173–2178.

Blasko, I., Marx, F., Steiner, E., Hartmann, T., Grubeck-Loebenstein, B., 1999. TNFalpha plus IFNgamma induce the production of Alzheimer beta-amyloid peptides and decrease the secretion of APPs. FASEB J. 13, 63–68.

Boissonneault, V., Filali, M., Lessard, M., Relton, J., Wong, G., Rivest, S., 2009. Powerful beneficial effects of macrophage colony-stimulating factor on beta-

amyloid deposition and cognitive impairment in Alzheimer's disease. Brain 132, 1078–1092.
Bonardi, C., de Pulford, F., Jennings, D., Pardon, M.-C., 2011. A detailed analysis of the early context extinction deficits seen in APPswe/PS1dE9 female mice and their relevance to preclinical Alzheimer's disease. Behav. Brain Res. 222, 89–97.
Bornemann, K.D., Wiederhold, K.H., Pauli, C., Ermini, F., Stalder, M., Schnell, L., Sommer, B., Jucker, M., Staufenbiel, M., 2001. Abeta-induced inflammatory processes in microglia cells of APP23 transgenic mice. Am. J. Pathol. 158, 63–73.
Bossers, K., Wirz, K.T.S., Meerhoff, G.F., Essing, A.H.W., van Dongen, J.W., Houba, P., Kruse, C.G., Verhaagen, J., Swaab, D.F., 2010a. Concerted changes in transcripts in the prefrontal cortex precede neuropathology in Alzheimer's disease. Brain 133, 3699–3723.
Bossers, K., Ylstra, B., Brakenhoff, R.H., Smeets, S.J., Verhaagen, J., van de Wiel, M.A., 2010b. Intensity-based analysis of dual-color gene expression data as an alternative to ratio-based analysis to enhance reproducibility. BMC Genomics 11, 112.
Braak, H., de Vos, R.A., Jansen, E.N., Bratzke, H., Braak, E., 1998. Neuropathological hallmarks of Alzheimer's and Parkinson's diseases. Prog. Brain Res. 117, 267–285.
Cahoy, J.D., Emery, B., Kaushal, A., Foo, L.C., Zamanian, J.L., Christopherson, K.S., Xing, Y., Lubischer, J.L., Krieg, P.A., Krupenko, S.A., Thompson, W.J., Barres, B.A., 2008. A transcriptome database for astrocytes, neurons, and oligodendrocytes: a new resource for understanding brain development and function. J. Neurosci. 28, 264–278.
Carro, E., Trejo, J.L., Gerber, A., Loetscher, H., Torrado, J., Metzger, F., Torres-Aleman, I., 2006. Therapeutic actions of insulin-like growth factor I on APP/PS2 mice with severe brain amyloidosis. Neurobiol. Aging 27, 1250–1257.
Carson-Walter, E.B., Watkins, D.N., Nanda, A., Vogelstein, B., Kinzler, K.W., St Croix, B., 2001. Cell surface tumor endothelial markers are conserved in mice and humans. Cancer Res. 61, 6649–6655.
Chen, K., Iribarren, P., Hu, J., Chen, J., Gong, W., Cho, E.H., Lockett, S., Dunlop, N.M., Wang, J.M., 2006. Activation of Toll-like receptor 2 on microglia promotes cell uptake of Alzheimer disease-associated amyloid beta peptide. J. Biol. Chem. 281, 3651–3659.
Davies, G., Cunnick, G.H., Mansel, R.E., Mason, M.D., Jiang, W.G., 2004. Levels of expression of endothelial markers specific to tumour-associated endothelial cells and their correlation with prognosis in patients with breast cancer. Clin. Exp. Metastasis. 21, 31–37.
DeKosky, S.T., Aston, C.E., Kamboh, M.I., 1996. Polygenic determinants of Alzheimer's disease: modulation of the risk by alpha-1-antichymotrypsin. Ann. N. Y. Acad. Sci. 802, 27–34.
Dickey, C.A., Gordon, M.N., Mason, J.E., Wilson, N.J., Diamond, D.M., Guzowski, J.F., Morgan, D., 2004. Amyloid suppresses induction of genes critical for memory consolidation in APP + PS1 transgenic mice. J. Neurochem. 88, 434–442.
Dickey, C.A., Loring, J.F., Montgomery, J., Gordon, M.N., Eastman, P.S., Morgan, D., 2003. Selectively reduced expression of synaptic plasticity-related genes in amyloid precursor protein + presenilin-1 transgenic mice. J. Neurosci. 23, 5219–5226.
Duan, R.S., Yang, X., Chen, Z.G., Lu, M.O., Morris, C., Winblad, B., Zhu, J., 2008. Decreased fractalkine and increased IP-10 expression in aged brain of APP(swe) transgenic mice. Neurochem. Res. 33, 1085–1089.
Eikelenboom, P., van Exel, E., Hoozemans, J.J.M., Veerhuis, R., Rozemuller, A.J.M., van Gool, W.A., 2010. Neuroinflammation - an early event in both the history and pathogenesis of Alzheimer's disease. Neurodegener. Dis. 7, 38–41.
Eikelenboom, P., Veerhuis, R., van Exel, E., Hoozemans, J.J.M., Rozemuller, A.J.M., van Gool, W.A., 2011. The early involvement of the innate immunity in the pathogenesis of late-onset Alzheimer's disease: neuropathological, epidemiological and genetic evidence. Curr. Alzheimer Res. 8, 142–150.
Emilsson, L., Saetre, P., Jazin, E., 2006. Alzheimer's disease: mRNA expression profiles of multiple patients show alterations of genes involved with calcium signaling. Neurobiol. Dis. 21, 618–625.
Fan, R., Xu, F., Previti, M.L., Davis, J., Grande, A.M., Robinson, J.K., Van Nostrand, W.E., 2007. Minocycline reduces microglial activation and improves behavioral deficits in a transgenic model of cerebral microvascular amyloid. J. Neurosci. 27, 3057–3063.
Filali, M., Lalonde, R., 2009. Age-related cognitive decline and nesting behavior in an APPswe/PS1 bigenic model of Alzheimer's disease. Brain Res. 1292, 93–99.
Fonseca, M.I., Chu, S.H., Berci, A.M., Benoit, M.E., Peters, D.G., Kimura, Y., Tenner, A.J., 2011. Contribution of complement activation pathways to neuropathology differs among mouse models of Alzheimer's disease. J. Neuroinflammation 8, 4.
Frank, S., Burbach, G.J., Bonin, M., Walter, M., Streit, W., Bechmann, I., Deller, T., 2008. TREM2 is upregulated in amyloid plaque-associated microglia in aged APP23 transgenic mice. Glia 56, 1438–1447.
Frank-Cannon, T.C., Alto, L.T., McAlpine, F.E., Tansey, M.G., 2009. Does neuroinflammation fan the flame in neurodegenerative diseases? Mol. Neurodegener. 4, 47.
Frankola, K.A., Greig, N.H., Luo, W., Tweedie, D., 2011. Targeting TNF-α to elucidate and ameliorate neuroinflammation in neurodegenerative diseases. CNS Neurol. Disord. Drug Targets 10, 391–403.
Galimberti, D., Schoonenboom, N., Scheltens, P., Fenoglio, C., Bouwman, F., Venturelli, E., Guidi, I., Blankenstein, M.A., Bresolin, N., Scarpini, E., 2006. Intrathecal chemokine synthesis in mild cognitive impairment and Alzheimer disease. Arch. Neurol. 63, 538–543.
Garcia-Alloza, M., Robbins, E.M., Zhang-Nunes, S.X., Purcell, S.M., Betensky, R.A., Raju, S., Prada, C., Greenberg, S.M., Bacskai, B.J., Frosch, M.P., 2006. Characterization of amyloid deposition in the APPswe/PS1dE9 mouse model of Alzheimer disease. Neurobiol. Dis. 24, 516–524.
Gasparini, L., Xu, H., 2003. Potential roles of insulin and IGF-1 in Alzheimer's disease. Trends Neurosci. 26, 404–406.
Gilchrist, M., Thorsson, V., Li, B., Rust, A.G., Korb, M., Roach, J.C., Kennedy, K., Hai, T., Bolouri, H., Aderem, A., 2006. Systems biology approaches identify ATF3 as a negative regulator of Toll-like receptor 4. Nature 441, 173–178.
Gimbel, D.A., Nygaard, H.B., Coffey, E.E., Gunther, E.C., Lauren, J., Gimbel, Z.A., Strittmatter, S.M., 2010. Memory impairment in transgenic Alzheimer mice requires cellular prion protein. J. Neurosci. 30, 6367–6374.
Hanisch, U.K., Kettenmann, H., 2007. Microglia: active sensor and versatile effector cells in the normal and pathologic brain. Nat. Neurosci. 10, 1387–1394.
Harvey, R.J., Skelton-Robinson, M., Rossor, M.N., 2003. The prevalence and causes of dementia in people under the age of 65 years. J. Neurol. Neurosurg. Psychiatr. 74, 1206–1209.
Hickman, S.E., Allison, E.K., El, K.J., 2008. Microglial dysfunction and defective beta-amyloid clearance pathways in aging Alzheimer's disease mice. J. Neurosci. 28, 8354–8360.
Holcomb, L., Gordon, M.N., McGowan, E., Yu, X., Benkovic, S., Jantzen, P., Wright, K., Saad, I., Mueller, R., Morgan, D., Sanders, S., Zehr, C., O'Campo, K., Hardy, J., Prada, C.M., Eckman, C., Younkin, S., Hsiao, K., Duff, K., 1998. Accelerated Alzheimer-type phenotype in transgenic mice carrying both mutant amyloid precursor protein and presenilin 1 transgenes. Nat. Med. 4, 97–100.
Hooijmans, C.R., Van der Zee, C.E.E.M., Dederen, P.J., Brouwer, K.M., Reijmer, Y.D., van Groen, T., Broersen, L.M., Lütjohann, D., Heerschap, A., Kiliaan, A.J., 2009. DHA and cholesterol containing diets influence Alzheimer-like pathology, cognition and cerebral vasculature in APPswe/PS1dE9 mice. Neurobiol. Dis. 33, 482–498.
Israelsson, C., Bengtsson, H., Lobell, A., Nilsson, L.N.G., Kylberg, A., Isaksson, M., Wootz, H., Lannfelt, L., Kullander, K., Hillered, L., Ebendal, T., 2010. Appearance of Cxcl10-expressing cell clusters is common for traumatic brain injury and neurodegenerative disorders. Eur. J. Neurosci. 31, 852–863.
Jankowsky, J.L., Fadale, D.J., Anderson, J., Xu, G.M., Gonzales, V., Jenkins, N.A., Copeland, N.G., Lee, M.K., Younkin, L.H., Wagner, S.L., Younkin, S.G., Borchelt, D.R., 2004. Mutant presenilins specifically elevate the levels of the 42 residue beta-amyloid peptide in vivo: evidence for augmentation of a 42-specific gamma secretase. Hum. Mol. Genet. 13, 159–170.
Jankowsky, J.L., Melnikova, T., Fadale, D.J., Xu, G.M., Slunt, H.H., Gonzales, V., Younkin, L.H., Younkin, S.G., Borchelt, D.R., Savonenko, A.V., 2005. Environmental enrichment mitigates cognitive deficits in a mouse model of Alzheimer's disease. J. Neurosci. 25, 5217–5224.
Janz, R., Südhof, T.C., Hammer, R.E., Unni, V., Siegelbaum, S.A., Bolshakov, V.Y., 1999. Essential roles in synaptic plasticity for synaptogyrin I and synaptophysin I. Neuron 24, 687–700.
Jarvis, K., Assis-Nascimento, P., Mudd, L.M., Montague, J.R., 2007. Beta-amyloid toxicity and reversal in embryonic rat septal neurons. Neurosci. Lett. 423, 184–188.
Johnston, H., Boutin, H., Allan, S.M., 2011. Assessing the contribution of inflammation in models of Alzheimer's disease. Biochem. Soc. Trans. 39, 886–890.
Kamboh, M.I., Minster, R.L., Kenney, M., Ozturk, A., Desai, P.P., Kammerer, C.M., DeKosky, S.T., 2006. Alpha-1-antichymotrypsin (ACT or SERPINA3) polymorphism may affect age-at-onset and disease duration of Alzheimer's disease. Neurobiol. Aging 27, 1435–1439.
Kamboh, M.I., Sanghera, D.K., Ferrell, R.E., DeKosky, S.T., 1995. APOE*4-associated Alzheimer's disease risk is modified by alpha 1-antichymotrypsin polymorphism. Nat. Genet. 10, 486–488.
Kamphuis, W., Orre, M., Kooijman, L., Dahmen, M., Hol, E.M., 2012. Differential cell proliferation in the cortex of the APPswePS1dE9 Alzheimer's disease mouse model. Glia 60, 615–629.
Kedra, D., Pan, H.Q., Seroussi, E., Fransson, I., Guilbaud, C., Collins, J.E., Dunham, I., Blennow, E., Roe, B.A., Piehl, F., Dumanski, J.P., 1998. Characterization of the human synaptogyrin gene family. Hum. Genet. 103, 131–141.
Khuu, C.H., Barrozo, R.M., Hai, T., Weinstein, S.L., 2007. Activating transcription factor 3 (ATF3) represses the expression of CCL4 in murine macrophages. Mol. Immunol. 44, 1598–1605.
Kilgore, M., Miller, C.A., Fass, D.M., Hennig, K.M., Haggarty, S.J., Sweatt, J.D., Rumbaugh, G., 2010. Inhibitors of class 1 histone deacetylases reverse contextual memory deficits in a mouse model of Alzheimer's disease. Neuropsychopharmacology 35, 870–880.
Labrousse, V.F., Nadjar, A., Joffre, C., Costes, L., Aubert, A., Grégoire, S., Bretillon, L., Layé, S., 2012. Short-term long chain omega3 diet protects from neuroinflammatory processes and memory impairment in aged mice. PLoS One 7, e36861.
Lagadec, S., Rotureau, L., Hémar, A., Macrez, N., Delcasso, S., Jeantet, Y., Cho, Y.H., 2012. Early temporal short-term memory deficits in double transgenic APP/PS1 mice. Neurobiol. Aging 33. 203.e1–11.
Li, C., Zhao, R., Gao, K., Wei, Z., Yin, M.Y., Lau, L.T., Chui, D., Hoi Yu, A.C., 2011. Astrocytes: implications for neuroinflammatory pathogenesis of Alzheimer's disease. Curr. Alzheimer Res. 8, 67–80.
Liang, W.S., Dunckley, T., Beach, T.G., Grover, A., Mastroeni, D., Ramsey, K., Caselli, R.J., Kukull, W.A., McKeel, D., Morris, J.C., Hulette, C.M., Schmechel, D., Reiman, E.M., Rogers, J., Stephan, D.A., 2010. Neuronal gene expression in non-demented individuals with intermediate Alzheimer's Disease neuropathology. Neurobiol. Aging 31, 549–566.
Liu, S., Liu, Y., Hao, W., Wolf, L., Kiliaan, A.J., Penke, B., Rübe, C.E., Walter, J., Heneka, M.T., Hartmann, T., Menger, M.D., Fassbender, K., 2012. TLR2 is

a primary receptor for Alzheimer's amyloid β peptide to trigger neuroinflammatory activation. J. Immunol. 188, 1098–1107.
Maier, M., Peng, Y., Jiang, L., Seabrook, T.J., Carroll, M.C., Lemere, C.A., 2008. Complement C3 deficiency leads to accelerated amyloid beta plaque deposition and neurodegeneration and modulation of the microglia/macrophage phenotype in amyloid precursor protein transgenic mice. J. Neurosci. 28, 6333–6341.
Melchior, B., Garcia, A.E., Hsiung, B.-K., Lo, K.M., Doose, J.M., Thrash, J.C., Stalder, A.K., Staufenbiel, M., Neumann, H., Carson, M.J., 2010. Dual induction of TREM2 and tolerance-related transcript, Tmem176b, in amyloid transgenic mice: implications for vaccine-based therapies for Alzheimer's disease. ASN Neuro. 2, e00037.
Melnikova, T., Savonenko, A., Wang, Q., Liang, X., Hand, T., Wu, L., Kaufmann, W.E., Vehmas, A., Andreasson, K.I., 2006. Cycloxygenase-2 activity promotes cognitive deficits but not increased amyloid burden in a model of Alzheimer's disease in a sex-dimorphic pattern. Neuroscience 141, 1149–1162.
Miller-Delaney, S.F.C., Lieberam, I., Murphy, P., Mitchell, K.J., 2011. Plxdc2 is a mitogen for neural progenitors. PLoS One 6, e14565.
Minkeviciene, R., Ihalainen, J., Malm, T., Matilainen, O., Keksa-Goldsteine, V., Goldsteins, G., Iivonen, H., Leguit, N., Glennon, J., Koistinaho, J., Banerjee, P., Tanila, H., 2008. Age-related decrease in stimulated glutamate release and vesicular glutamate transporters in APP/PS1 transgenic and wild-type mice. J. Neurochem. 105, 584–594.
Mustafa, A., Lannfelt, L., Lilius, L., Islam, A., Winblad, B., Adem, A., 1999. Decreased plasma insulin-like growth factor-I level in familial Alzheimer's disease patients carrying the Swedish APP 670/671 mutation. Dement. Geriatr. Cogn. Disord. 10, 446–451.
Olabarria, M., Noristani, H.N., Verkhratsky, A., Rodríguez, J.J., 2010. Concomitant astroglial atrophy and astrogliosis in a triple transgenic animal model of Alzheimer's disease. Glia 58, 831–838.
O'Leary, T.P., Brown, R.E., 2009. Visuo-spatial learning and memory deficits on the Barnes maze in the 16-month-old APPswe/PS1dE9 mouse model of Alzheimer's disease. Behav. Brain Res. 201, 120–127.
Parachikova, A., Agadjanyan, M.G., Cribbs, D.H., Blurton-Jones, M., Perreau, V., Rogers, J., Beach, T.G., Cotman, C.W., 2007. Inflammatory changes parallel the early stages of Alzheimer disease. Neurobiol. Aging 28, 1821–1833.
Parachikova, A., Cotman, C.W., 2007. Reduced CXCL12/CXCR4 results in impaired learning and is downregulated in a mouse model of Alzheimer disease. Neurobiol. Dis. 28, 143–153.
Park, K.M., Bowers, W.J., 2010. Tumor necrosis factor-alpha mediated signaling in neuronal homeostasis and dysfunction. Cell Signal. 22, 977–983.
Paul, E., Pozdnyakova, O.O., Mitchell, E., Carroll, M.C., 2002. Anti-DNA autoreactivity in C4-deficient mice. Eur. J. Immunol. 32, 2672–2679.
Pillay, N.S., Kellaway, L.A., Kotwal, G.J., 2008. Early detection of memory deficits and memory improvement with vaccinia virus complement control protein in an Alzheimer's disease model. Behav. Brain Res. 192, 173–177.
Reddy, P.H., McWeeney, S., Park, B.S., Manczak, M., Gutala, R.V., Partovi, D., Jung, Y., Yau, V., Searles, R., Mori, M., Quinn, J., 2004. Gene expression profiles of transcripts in amyloid precursor protein transgenic mice: up-regulation of mitochondrial metabolism and apoptotic genes is an early cellular change in Alzheimer's disease. Hum. Mol. Genet. 13, 1225–1240.
Richard, K.L., Filali, M., Préfontaine, P., Rivest, S., 2008. Toll-like receptor 2 acts as a natural innate immune receptor to clear amyloid beta 1-42 and delay the cognitive decline in a mouse model of Alzheimer's disease. J. Neurosci. 28, 5784–5793.
Rmali, K.A., Puntis, M.C.A., Jiang, W.G., 2007. Tumour-associated angiogenesis in human colorectal cancer. Colorectal Dis. 9, 3–14.
Rolls, A., Shechter, R., London, A., Ziv, Y., Ronen, A., Levy, R., Schwartz, M., 2007. Toll-like receptors modulate adult hippocampal neurogenesis. Nat. Cell Biol. 9, 1081–1088.
Rozen, S., Skaletsky, H.J., 2000. Primer3 on the WWW for general users and for biologist programmers. In: Krawetz, S., Misener, S. (Eds.), Bioinformatics Methods and Protocols: Methods in Molecular Biology. Humana Press, Totowa, NJ, pp. 365–386.
Ruan, L., Kang, Z., Pei, G., Le, Y., 2009. Amyloid deposition and inflammation in Appswe/Ps1de9 mouse model of Alzheimer's disease. Curr. Alzheimer Res. 6, 531–540.
Sabroe, I., Dower, S.K., Whyte, M.K.B., 2005. The role of Toll-like receptors in the regulation of neutrophil migration, activation, and apoptosis. Clin. Infect. Dis. 41 (suppl 7), S421–S426.
Savonenko, A., Xu, G.M., Melnikova, T., Morton, J.L., Gonzales, V., Wong, M.P., Price, D.L., Tang, F., Markowska, A.L., Borchelt, D.R., 2005. Episodic-like memory deficits in the APPswe/PS1dE9 mouse model of Alzheimer's disease: relationships to beta-amyloid deposition and neurotransmitter abnormalities. Neurobiol. Dis. 18, 602–617.
Selwood, S.P., Parvathy, S., Cordell, B., Ryan, H.S., Oshidari, F., Vincent, V., Yesavage, J., Lazzeroni, L.C., Murphy Jr., G.M., 2009. Gene expression profile of the PDAPP mouse model for Alzheimer's disease with and without apolipoprotein E. Neurobiol. Aging 30, 574–590.
Smith, K.G.C., Clatworthy, M.R., 2010. FcgammaRIIB in autoimmunity and infection: evolutionary and therapeutic implications. Nat. Rev. Immunol. 10, 328–343.
Smyth, G.K., 2004. Linear models and empirical bayes methods for assessing differential expression in microarray experiments. Stat. Appl. Genet. Mol. Biol. 3. Article3.
Standiford, T.J., Kuick, R., Bhan, U., Chen, J., Newstead, M., Keshamouni, V.G., 2011. TGF-β-induced IRAK-M expression in tumor-associated macrophages regulates lung tumor growth. Oncogene 30, 2475–2484.
Sugita, S., Janz, R., Südhof, T.C., 1999. Synaptogyrins regulate Ca2+-dependent exocytosis in PC12 cells. J. Biol. Chem. 274, 18893–18901.
Thomas, D.M., Francescutti-Verbeem, D.M., Kuhn, D.M., 2006. Gene expression profile of activated microglia under conditions associated with dopamine neuronal damage. FASEB J. 20, 515–517.
Timmer, N.M., van, D.L., Van der Zee, C.E., Kiliaan, A., De Waal, R.M., Verbeek, M.M., 2010. Enoxaparin treatment administered at both early and late stages of amyloid beta deposition improves cognition of APPswe/PS1dE9 mice with differential effects on brain A beta levels. Neurobiol. Dis. 40, 340–347.
Toledo, E.M., Inestrosa, N.C., 2010. Activation of Wnt signaling by lithium and rosiglitazone reduced spatial memory impairment and neurodegeneration in brains of an APPswe/PSEN1DeltaE9 mouse model of Alzheimer's disease. Mol. Psychiatry. 15, 272–285. 228.
Torres-Aleman, I., 2000. Serum growth factors and neuroprotective surveillance: focus on IGF-1. Mol. Neurobiol. 21, 153–160.
Vandesompele, J., De Preter, K., Pattyn, F., Poppe, B., Van Roy, N., De Paepe, A., Speleman, F., 2002. Accurate normalization of real-time quantitative RT-PCR data by geometric averaging of multiple internal control genes. Genome Biol. 3. RESEARCH0034.
Wisniewski, T., Sigurdsson, E.M., 2010. Murine models of Alzheimer's disease and their use in developing immunotherapies. Biochim. Biophys. Acta. 1802, 847–859.
World Health Organization, Alzheimer's Disease International, 2012. Dementia: a public health priority. WHO Press, Geneva, Switzerland.
Wu, Z.L., Ciallella, J.R., Flood, D.G., O'Kane, T.M., Bozyczko-Coyne, D., Savage, M.J., 2006. Comparative analysis of cortical gene expression in mouse models of Alzheimer's disease. Neurobiol. Aging 27, 377–386.
Wyss-Coray, T., Loike, J.D., Brionne, T.C., Lu, E., Anankov, R., Yan, F., Silverstein, S.C., Husemann, J., 2003. Adult mouse astrocytes degrade amyloid-beta in vitro and in situ. Nat. Med. 9, 453–457.
Wyss-Coray, T., Yan, F., Lin, A.H.T., Lambris, J.D., Alexander, J.J., Quigg, R.J., Masliah, E., 2002. Prominent neurodegeneration and increased plaque formation in complement-inhibited Alzheimer's mice. Proc. Natl. Acad. Sci. U. S. A 99, 10837–10842.
Xu, P.T., Li, Y.J., Qin, X.J., Scherzer, C.R., Xu, H., Schmechel, D.E., Hulette, C.M., Ervin, J., Gullans, S.R., Haines, J., Pericak-Vance, M.A., Gilbert, J.R., 2006. Differences in apolipoprotein E3/3 and E4/4 allele-specific gene expression in hippocampus in Alzheimer disease. Neurobiol. Dis. 21, 256–275.
Yan, P., Bero, A.W., Cirrito, J.R., Xiao, Q., Hu, X., Wang, Y., Gonzales, E., Holtzman, D.M., Lee, J.M., 2009. Characterizing the appearance and growth of amyloid plaques in APP/PS1 mice. J. Neurosci. 29, 10706–10714.
Yao, S., Wang, S., Zhu, Y., Luo, L., Zhu, G., Flies, S., Xu, H., Ruff, W., Broadwater, M., Choi, I.H., Tamada, K., Chen, L., 2009. PD-1 on dendritic cells impedes innate immunity against bacterial infection. Blood 113, 5811–5818.
Yu, J.T., Mou, S.M., Wang, L.Z., Mao, C.X., Tan, L., 2011. Toll-like receptor 2 -196 to -174 del polymorphism influences the susceptibility of Han Chinese people to Alzheimer's disease. J. Neuroinflammation 8, 136.
Zhang, W., Bai, M., Xi, Y., Hao, J., Zhang, Z., Su, C., Lei, G., Miao, J., Li, Z., 2012. Multiple inflammatory pathways are involved in the development and progression of cognitive deficits in APPswe/PS1dE9 mice. Neurobiol. Aging 33, 2661–2677.
Zota, V., Nemirovsky, A., Baron, R., Fisher, Y., Selkoe, D.J., Altmann, D.M., Weiner, H.L., Monsonego, A., 2009. HLA-DR alleles in amyloid beta-peptide autoimmunity: a highly immunogenic role for the DRB1*1501 allele. J. Immunol. 183, 3522–3530.